Geomechanical and Geochemical impact of CO$_2$ injection at the North Sea Cranberry Opportunity

Lidewij Schutte (3921530)
Utrecht University
Master Earth Structure and Dynamics
Master thesis
21/02/2019
1st Supervisor: Dr. S.J.T. Hangx
2nd Supervisor: S. Bottero, PhD
3rd Supervisor: Prof. Dr. J.H.P. de Bresser
4th Supervisor: Prof. C.J. Spiers

Utrecht University

Abstract

In an effort to reduce CO_2 emissions, but still provide society with much used natural gas, Circular Energy wants to simultaneously produce natural gas and inject CO_2, that is a result from production of electricity from natural gas. The effects of CO_2 injection are researched, but not injection in a still full reservoir. Effects that need further research are dissolution of minerals, fluid-rock ratio, strain due to simultaneous production and injection, increased stress around the well bore due to delayed pressure distribution, possible injection into an aquifer and the precipitation of minerals, especially around the injection well bore, which would decrease permeability. Options to look into several of these effects are reactive transport modelling and reservoir modelling. Basic calculations indicate that the strength of the reservoir is high enough to produce natural gas and to inject CO_2 at the onset. However the parameters used are hypothetical and the effective stress was not looked into. Especially ongoing injection might cause problems of unsure nature. Basic calculations indicate that flexural bending is probably not a severe effect as the maximum expected compaction is 3 cm and that due to the simultaneous injection the pores will not empty completely.

1. Table of Contents

2. Introduction

In view of increased efforts to make the energy market more sustainable and as a tie in to the energy transition (United Nations Treaty Collect, 2015), it is envisioned that it is possible to produce natural gas simultaneously with the storage of CO_2, which is produced during electricity generation from the natural gas. The energy transition is the transition from a hydrocarbon based energy supply to a green and sustainable energy supply. The electricity will be generated on the production site. This will lead to a closed and localised energy system as there is no CO_2 emission into the atmosphere. There is no influx of CO_2 onto the production site from the mainland, so all the CO_2 stored on site is produced on site. CO_2 produced on the mainland is not transported to the production site for storage. It is expected that the energy transition will take at least a few decades. If this closed system is directed at smaller gas accumulations that can be completed in a decade and are currently not connected to existing gas infrastructure, the idea is economically feasible.

The production of natural gas as a fossil fuel for electricity is a common practice in the Netherlands. Natural gas has a lower CO_2 emission compared to coal and oil. Therefore this relatively 'clean' fossil fuel is envisioned to help in the energy transition. As the Groningen field is envisioned to cease producing, the focus of gas production activities is stimulated to focus on small offshore fields (Wiebes, 2018). To further reduce the amount of CO_2 emission, CO_2 Capture and Storage (CCS) is expected to play a significant role in the Netherlands. By combining the policy of focussing on exploiting small gas fields and the expected developing of CCS, a possibility has arisen for developing electricity generation on site with natural gas and use CCS to reduce the CO_2 emission and thus creating a circular energy system. However, both production of gas and injection of CO_2 may lead to a range of geomechanical and geochemical effects, as both take the subsurface system out of physical and chemical equilibrium. CCS is being under investigation, as it has unknown effects long term, and is being done commercially (Torp & Gale, 2004). First production and then storage in the same field has been done before, the production and storage of methane and CO_2 simultaneously from the onset of production, however is a completely new concept. As such unknown geomechanical and/or geochemical effects can occur with possibly negative results. A concern is the stability of the caprock during initial injection, because of potential fracturing due to too much overpressure and possible surface subsidence due to production.

The production of natural gas is well developed, though prolonged gas production may lead to negative side-effects, like surface subsidence (Hettema *et al.* (2000), Hol *et al.*, 2015), induced seismicity (NAM, 2013) and ongoing reservoir compaction even after production has stopped (Eysink *et al.*, 2000). It is believed that these processes are driven by the increase in effective stress state acting on the reservoir as the pore pressure reduces due to production, leading to compaction at the reservoir level. Significant compaction of the reservoir could lead to flexural bending of the overlying caprock, and potentially the creation of small fractures at the base of the caprock (Hangx *et al.*, 2010-AB). However, these effects could likely be reduced by pressure maintenance of the reservoir, either by the injection of water, CO_2 or other high pressure fluids. It is of interest to look into short term compaction, if the reservoir has a low permeability and the injected fluids will take longer to spread.

Injection of high pressure CO_2, and the subsequent long-term subsurface storage, has the additional benefit that it aids in reducing global CO_2 emissions (Bachu, 2008). The proposed idea does not reduce the amount of CO_2 in the atmosphere. As stated by Bachu (2003), sedimentary basins are suitable for CO_2 storage, particularly depleted oil and gas reservoirs, and deep carbonate and sandstone aquifers. While pressurised aquifers may pose risks due to potential over pressuring during CO_2 injection (Michael *et al.*, 2010), depleted or depleting hydrocarbon reservoirs may not have this problem. However, dissolution of injected CO_2 into reservoir brine will create an acid

environment, which could lead to dissolution of primary minerals and precipitation of new minerals. These chemical changes to the rock matrix could impact the mechanical behaviour of the reservoir and caprock (Röhmer *et al.*, 2016), which in turn may affect the storage integrity of the system. As such, an in depth examination of possible effects is necessary.

For field development, it is important to assess the impact of gas production on one end of the field and CO_2 injection on the other end. The field needs to be assessed for its storage capacity for CO_2, and how this is affected by potential reservoir compaction and heave, and sealing integrity, which in turn may be affected by fluid/rock interactions and pressure changes induced by production and injection. Injection in an overpressured gas reservoir might cause damage to the reservoir and sealing rock and might induce a loss of containment. Possible causes can include micro fractures and diffusion in the caprock. This can cause leakage of CO_2 and methane into the overlying rock formations. If the overburden has for example parts carbonate and anhydrite cementation, this cementation might (partially) dissolve and weaken the rock. In the reservoir itself, the dissolution of carbonate and anhydrite cement is of interest as well, with a view to reservoir rock stability. In addition to dissolution, the precipitation of minerals and clogging of pores is an important effect as well. Important for clogging and flow effects is the expected CO_2 flow path to the top of the reservoir (Gaus, 2010) as CO_2 is lighter than methane and CO_2 and methane differ in relative permeability which results in CO_2 bypassing methane. These effects might reduce the injection rates of the CO_2 as they reduce the permeability and porosity.
For this assessment, knowledge of the field (geology, structure) is needed as well the impact of pressure, temperature and chemical changes on its behaviour. Regarding the latter, much can be learned from existing studies on producing hydrocarbon fields, such as the Groningen gas field, and research into carbon capture and storage (for example, Hangx *et al.* (2015), Heinemann *et al.* (2013)).

The main objective of this project is to assess the potential effects of simultaneous gas production from and CO2 injection into a single reservoir. This assessment is performed for the Cranberry Opportunity, located offshore in the Dutch North Sea, but the approach can be applied to other potential locations targeted for combined methane production and CO_2 storage. In addition to an overview of potential chemical and mechanical effects resulting from production and/or injection, the impact of pressure changes on the mechanical integrity of the reservoir-caprock system was quantified through predictions in the changes in the state of stress and the extent of flexural bending of the caprock.

3. Field characteristics

As implementation of this ambitious plan depends on the suitability of the chosen field, characteristics of said field need to be taken into consideration. Firstly and most easy is to look into the suitability for production. Secondly and more difficult is to look into the suitability for injection. However before determining the suitability, looking into the field characteristics is a first step.

3.1. Geological setting

In order to determine the suitability of the offshore region in the Netherlands for this type of project, information about the geological and tectonic setting is required. To avoid fault reactivation, a region should not be tectonically active. The Dutch subsurface and offshore subsurface have a high potential for gas reservoirs. Most of these reservoirs have been scouted, but new discoveries are still made, for example the offshore field Gems. (DvhN, 2017) In order to explain this high potential, a concise geological history will be presented.

Most reservoirs are located in Permian Rotliegend sandstones and Bunter Sandstone from the Triassic. The Cranberry Opportunity is located in the Permian Rotliegend sandstone as are numerous other gas accumulations such as the Slochteren natural gas field. Our focus will be on the Permian sandstone. This suitability for gas accumulations is caused by the depositional environment during the Permian (Wong *et al.*, 2007). Permian deposits are arranged in three parts: Lower and Upper Rotliegend and Zechstein (Wong *et al.*, 2007). From the Early Permian no sediments are left in the

Figure 1 Facies distribution at the onset of the deposition of the Upper Slochteren Member. (Taken from Wong et al. 2007, who made it after Lokhorst, 1998) TIJH: Texel-IJsselmeer High; MNSH: Mid North Sea High; RFH: Ringkøbing-Fyn High

Dutch subsurface. Lower Rotliegend is from Middle Permian times and are volcanic in origin and are of no interest as reservoirs as these volcanic depositions contain no producible gas (Wong *et al.*, 2007). Upper Rotliegend and Zechstein are Middle and Late Permian in origin (Wong *et al.*, 2007). The Zechstein formation is for most natural gas fields the caprock, primary or secondary, as it consists mostly of marine evaporites and carbonates, which have a low permeability and low porosity. Upper Rotliegend rocks were deposited in warm and dry conditions and environments are determined to be fluvial, aeolian and playa lake (Figure 1) (Wong *et al.*, 2007).
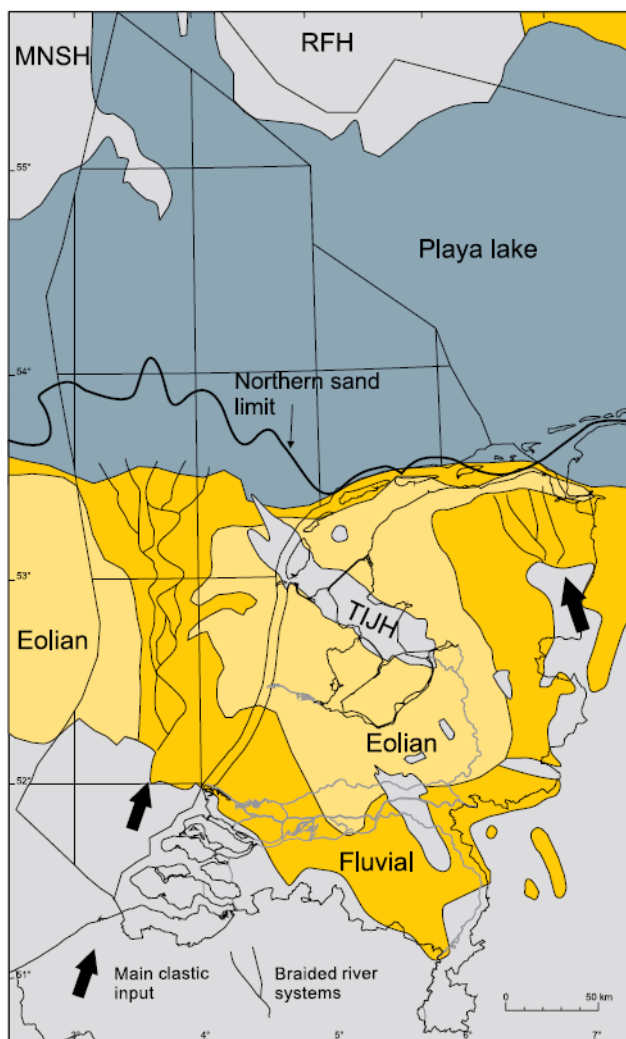
The playa lake deposits are mostly found in the northern offshore area. Most reservoirs are found in Upper Rotliegend rocks as the depositional environment, such as eolian, playa lake or fluvial which deposit mostly

sands, was optimal for creating possible reservoir rock as they consist of sandstones (Wong *et al.*, 2007). Sandstones are suitable as a reservoir rock because of the higher porosities and permeabilities. The first tectonics that impacted the Rotliegend formation are the last remnants of the Variscan Orogeny and thus are convergent (Wong *et al.*, 2007). The resulting faults were later inverted.
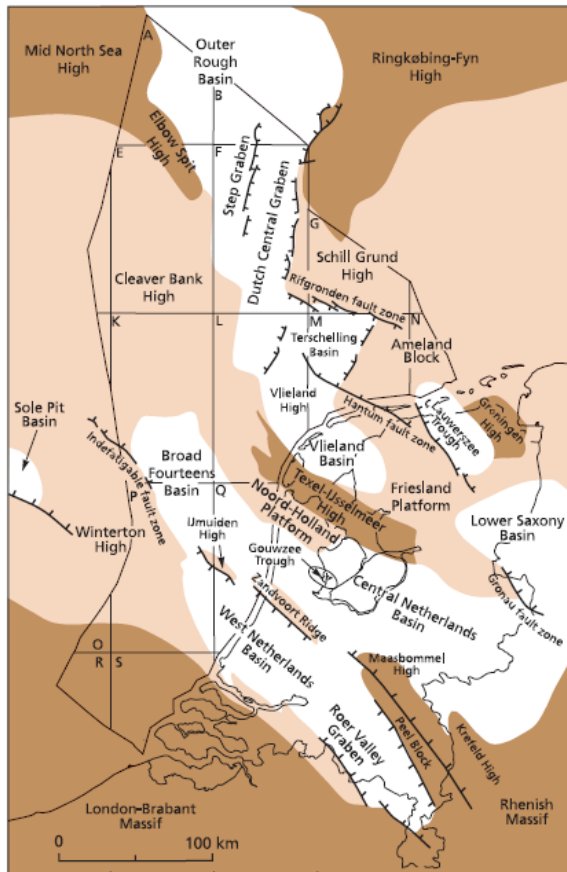

Figure 2 Structural elements in the Netherlands up until the Early Cretaceous. (from Wong et al., 2007) Dark brown: structural high, partly subaerial landmass; light brown: platform, intermittently flooded; white: basin.

During the Triassic two phases of tectonic extension occurred which are linked to the break-up of Pangea. The first, Hardegsen phase, mostly affected the deposition and sediments of the Buntsandstein. The second, Early Kimmerian, mainly affected Triassic Groups overlying the Permian sandstones (Wong *et al.*, 2007). The Permian basins were initially preserved during the onset of rifting, but ongoing extension started to affect the basin configuration during the Triassic. Rifts are found through the Southern Permian Basin. In the Netherlands gentle faulting is thought to impact the already deposited youngest sediments during the Triassic (Wong *et al.*, 2007). During the Triassic the Horn Grabens were formed to the north of Germany. The Hardegsen and Early Kimmerian extensions were mostly east-west oriented. This ongoing faulting penetrated through the basement and was the onset of the movement of Zechstein salts (Wong *et al.*, 2007).

Rifting continued into the Jurassic. This resulted in the break-up of the Southern Permian Basin into several smaller basins and highs located across the Netherlands, which are bounded by faults (Wong *et al.*, 2007). Like the Triassic, the Jurassic also has two phases of extension: Mid and Late Kimmerian phases. At the end of the Jurassic the subsurface can be divided into three smaller structural provinces: the north-south striking Dutch Central Graben, the east-west striking Lower Saxony Basin and the northwest-southeast striking system of Roer Vally Graben and Broad Fourteens Basin (Figure 2) (Wong *et al.*, 2007).

During the Cretaceous, the extensive rifting slowly ceased and changed into regional subsidence due to sagging. However, during the Late Cretaceous a short bout of inversion tectonics was observed. However, this inversion does not seem to affect the Permian sediments (Wong *et al.*, 2007). During the Tertiary these inversion tectonics were renewed, which is believed to be the result of the Laramide phase of the Alpine Orogeny (Wong *et al.*, 2007). According to Sissingh (2006) the Roer Valley Graben (oriented NW-SE) originate from the Rhine Graben (oriented NE-SW), which developed during the Eocene and Oligocene as a part of a major rift system. As this system developed more to the southeast, it is believed that the impact on the offshore are of the Netherlands is limited. After a

period of uplift in the Late Eocene, in the Late Oligocene subsidence was believed to be resumed and is ongoing. (Van Balen *et al* (2005)

The subsurface is characterized by an extensional regime, in spite of being first subjected to a short late stage of the Variscan Orogeny. The Late Jurassic and Early Cretaceous rift tectonics are most important to the present day structure of the subsurface. These inverted the earlier formed faults from the Variscan Orogeny, created more basins and uplift next to these basins and the special spread of salt can be linked to this time period as well.

3.2. Field Specifics

To determine whether a field is suitable for exploitation and with respect to this project sequestration, it is important to know various specifics of the field which is of interest. Such specifics include porosity, permeability, temperature, pressure situation, state of stress and depth as basic characteristics. Further specifics of interest are the composition of the brine, strength of the caprock and reservoir rock, composition of the gas and variation in permeability and porosity. These parameters can be used as input into preliminary calculations such as described in the chapters Failure Criterion and Flexural Bending and after the preliminary stage in building a reservoir model to model the behaviour of the reservoir.

From the Cranberry Opportunity the following specifics are known:

- Porosity — 8,5 - 9,8 % on average. Spread is 1,9 – 24,6 %.
- Permeability — <0.01 – 55.65 mD (average 1.33 mD)
- Temperature — 102 °C (375K)
- Overburden — 60,6 MPa at a depth of 2687 m based on a density of 2300 kg/m3
- State of stress — Unknown (World Stress Map) Could be extensional, because of normal faults.
- Depth (reservoir) — 2572 – 2705 m (133 m thick)
- Gas bearing layer — 2572 – 2636 m (64 m)
- Gas composition — 75% CH_4, 15% CO_2, 6% N_2 and 3% C_2H_6. Remaining 1% consists of a wide variety of gasses.
- Composition of brine — Unknown. Average from the region listed in Table 1

Cation/Anion	Concentration (mg/l)
Na+	80.933
K+	2233
NH4 +	160
Ca2 +	22.097
Mg2 +	2343
Sr2 +	625
Ba2 +	19
Pb2 +	28
Zn2 +	125
Total Fe	323
Cl–	173.648
SO42 –	203
HCO3–	1400

Table 1 Average fluid composition (mg/l) from the NE Netherlands for Rotliegend reservoir sandstones. Data were provided by NAM. (Taken from Waldmann et al., 2014)

The Cranberry opportunity is situated in a horst block bounded by faults on three sides (Figure 3). The SE boundary is defined by a dip closure. (Fact sheet, 2006, Ministry of Economic Affairs) Preferably CO_2 injection takes place in locations of low tectonic activity. Highly tectonically active regions might increase the potential of reactivation of binding faults.

For the time being, a decision has not yet been made to either inject in the gas part of a reservoir or aquifer/water bearing layer.
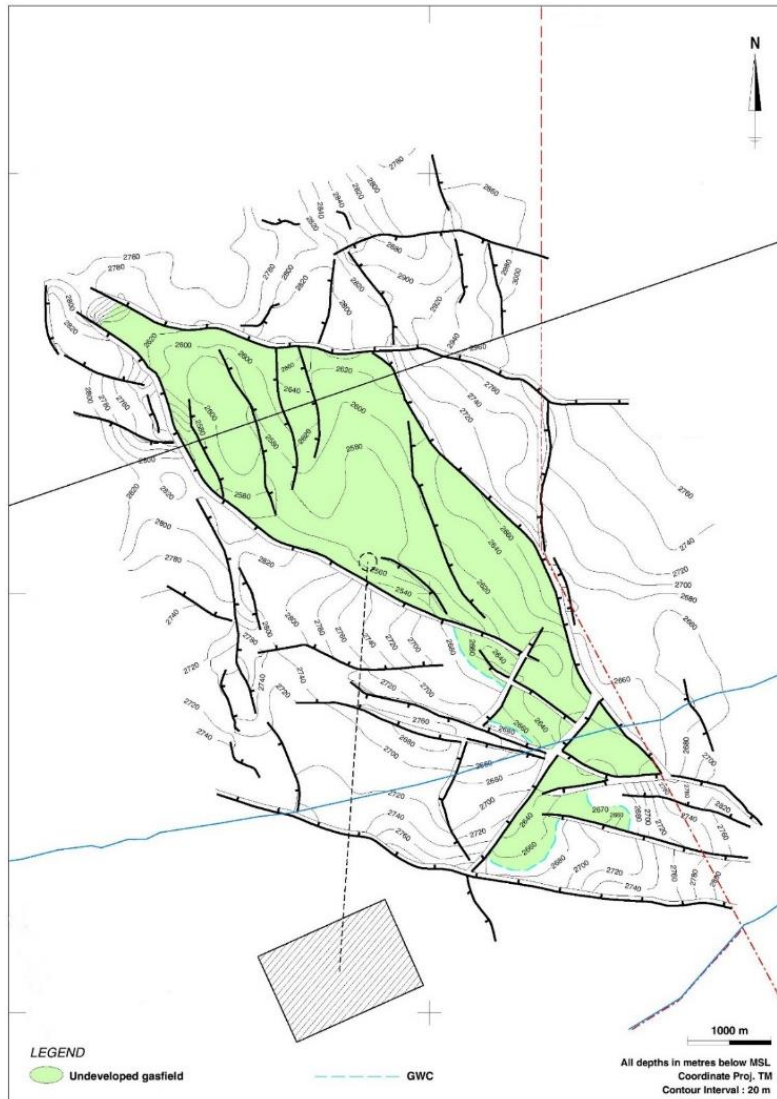
Figure 3 Top view of the Cranberry Opportunity (Taken from Nlog)

The following lithostratigraphic column (Table 2) is known for the Cranberry Opportunity. The measurements are taken 'along hole' and are not the true vertical depths as the borehole has a deviation. The deviation data stated that 2460-3005 m AH is equal to 2402-2890 m TVD. (Nlog.nl)

Stratigraphic unit	Top (m AH)	Bottom (m AH)
Zechstein caprock	2489	2519
Z2 Basal Anhydrite Member	2519	2555
Z2 Carbonate Member	2555	2568
Z1 Anhydrite Member	2568	2589
Z1 Carbonate Member	2589	2597
Coppershale Member	2597	2599
Ten Boer Member	2599	2686
Upper Slochteren Member	2686	2834
Buren Member	2834	2943

Table 2 Lithostratigraphic column for the Cranberry Opportunity. (Taken from Nlog.nl)

3.3. CO$_2$ characteristics

When dealing with CO$_2$ injection, it is important to realize that CO$_2$ has different characteristics than methane. As such a few characteristics will be highlighted here for easy access. In Figure 4 the phase
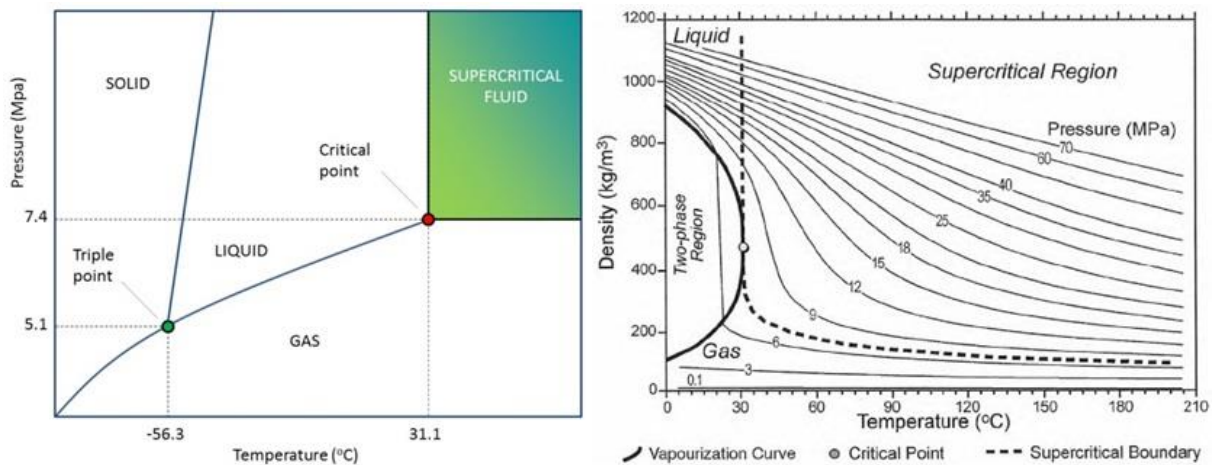

Figure 4 and Figure 5 Phase diagram of CO$_2$ and density of CO$_2$ at various temperatures and pressures. (Taken from www.scimed.co.uk)

diagram of CO$_2$ is presented. As most of the gas reservoirs are situated in the Permian sandstones

and those reside often at a depth of 2000 m or more, the CO$_2$ is almost always injected in the supercritical phase. In Figure 4 a graph is presented that depicts the density of CO$_2$ at different temperatures and pressures. This information can be used to predict the location of the injected CO$_2$ in the reservoir with respect to the methane and therefore also in modelling CO$_2$ in a reservoir. Khan *et al.* (2013) states that at a wide variety of reservoir conditions, CO$_2$ was 2-6 times more dense that methane.
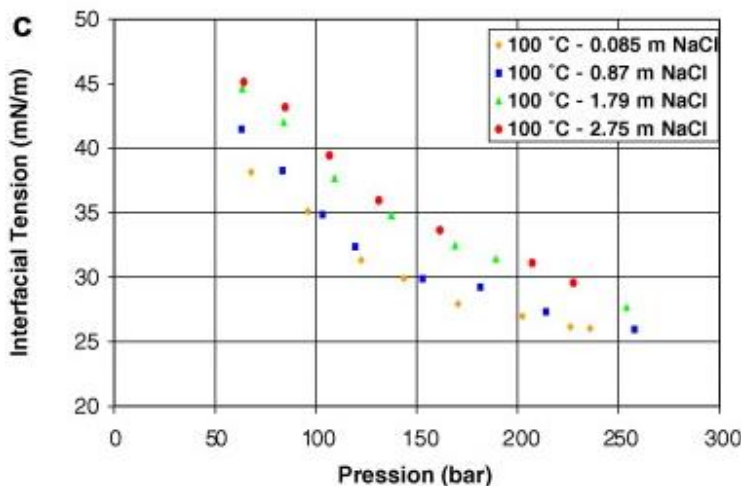
Figure 6 Interfacial tension at different pressures for fluids with different salinities. (T=100°C) (Taken from Chalbaud et al., 2009)

Another interesting characteristic would be interfacial tension. Interfacial tension describes the degree of how 'sticky' a substance is. It is also called surface tension.

As seen in Figure 6 the interfacial tension reduces when the pressure increases and that the interfacial tension is higher when the fluid has a higher salinity. Figure 7 shows similar information as Figure 6, however the first uses water with methane and CO$_2$ and the second uses brines. Figure 7 shows that adding CO$_2$ to methane and water, reduces the interfacial tension. In Figure 6 the graph of the lowest molarity, depicted in yellow, hints at a slightly exponential graph. This would suggest that 20 – 25 mN/m could be the range of lowest interfacial tension possible.
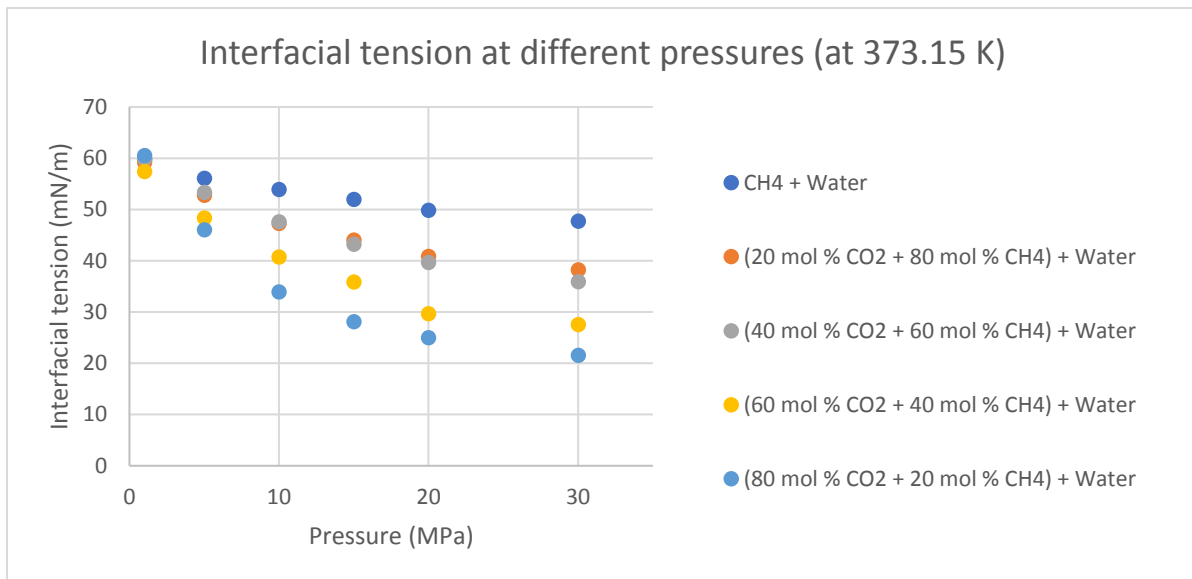
Figure 7 Interfacial tension of fluids with a different composition of CO_2 and CH_4 at varying pressures and a set temperature. (100°C) (Data taken from table 1 in Ren et al., 2000)

Next to phase information and changes in interfacial tension, solubility of CO_2 is also an interesting piece of information. It is interesting, because CO_2 can also be injected in an aquifer instead of an empty gas/oil reservoir. Both Duan *et al.* (2006) and Duan&Sun (2003) presented thermodynamic models to determine the solubility of CO_2 in various fluids, such as pure water and brines with different compositions and salinities. Two examples are presented in Figure 8. The model can be downloaded from http://www.geochem-model.org/programs.htm (Duan *et al.,* 2006).

Figure 8 Solubility of CO_2 in aqueous NaCl to the left and in pure water to the right. (Taken from Duan&Sun, 2003)

3.4. Petrophysical properties of reservoir and caprock

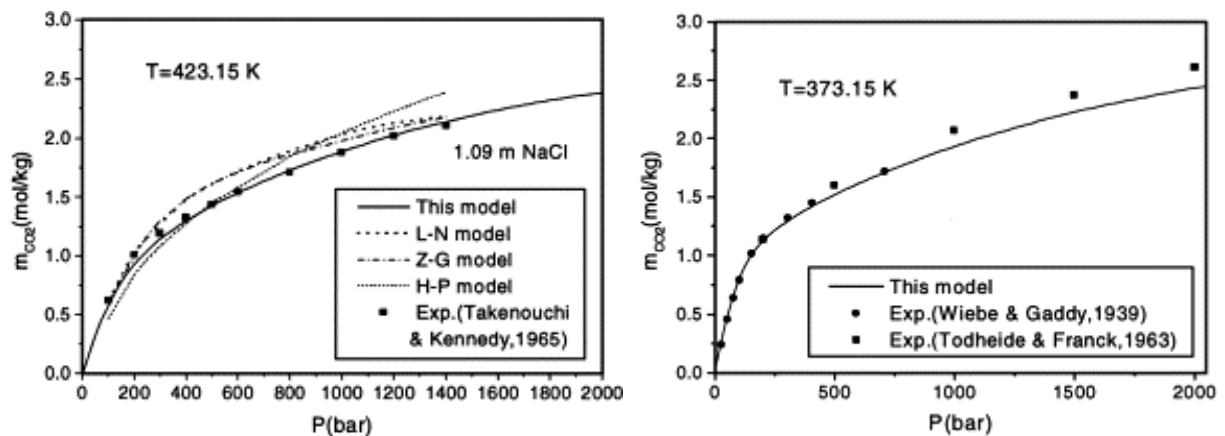| Quartz	Plag Fs	Dolomite	Siderite	Calcite	Anhydrite	Dawsonite	Halite	Hematite	Illite/Smectite	Kaolinite
58	3	8	4	0	0	2	tr	0	25	0
45	10	5	3	0	16	2	0	0	19	0
42	3	1	tr		3	1	3	1	46	0
60	2	9	3	0	tr	2	0	0	24	0
58	5	2	3	0	2	3	4	0	23	0
47	2	0	3	0	16	3	0	0	29	0
59	4	14	5	0	7	5	0	0	5	1
45	8	0	1	0	10	1	0	0	35	0
56	4	0	1	tr	11	1	0	0	27	0
46	3	15	5	0	19	1	0	0	8	3

Table 3 Whole rock mineralogy as determined with X-ray diffraction on 10 core samples, taken along the whole core. (Data taken from Nlog.nl)

Illite and smectite are taken as one type of clay as these signatures are very close. According to Horsrud *et al* (1999) somewhere between 2000 and 2600 m smectite is not present anymore. As this data is from even deeper, the expectation is that all illite/smectite is in fact illite and there is no smectite remaining.

Plug	Porosity	Primary porosity	Secondary porosity	Detrital Clays	Feldspar	Plagioclase	Anhydrite	Dolomite	Quartz	Secondary Kaolinite	K-feldspar	Siderite
26	10.2	8.7	1.5	16.7	10.6	6.6	cement	8.3				
59	12.2	7.4	4.8	13.3	6.7	4.4	cement	7.3	2.3	2.4		
76	4.2	3.2	1	44	11	5.3	1				5.7	
78	14.5	12	2.6	15.3	9.7	6.4	3	11.7			3.3	
122	9.4	3	6.3	20.6	6	4.7	7.7	9.3			1.3	0.7
131	6.3	2.2	4.1	27	3.7	2.4	7.7	5.7			1.3	
Plate 19A	18.3	14.2	4.1	0.3	13	8.3	2	10.3			4.7	
201	7.7	3.4	4.3	38.7	5.7	5	5.7				0.7	
223	2.3			25.3	7.3	5	5.7				0.3	2.6
248	11	4.2	6.8	7.3	8.3	6.6	8.4	14			1.7	3
Average	9.61	6.477778	3.944444	20.85	8.2	5.47	5.15	9.514286	2.3	2.4	2.375	2.1

Table 4 Percentages of minerals are taken from thin section analysis. (Data taken from Nlog.nl)

The above tables represent data from our example reservoir Cranberry. Important features include the amount of calcite present, as that can dissolve faster in more acidic fluids, amount of clays, as a high percentage can indicate a less permeable reservoir and with a lower porosity. Hematite is also susceptible for dissolution and after the dissolution of anorthite kaolinite together with calcite can precipitate.

The thin sections contained relatively high amounts of detrital clays. The cement minerals were determined to be dolomite, anhydrite and dawsonite. The quartz crystals have line contacts instead of point contact, which indicates pressure solution.

Depositional setting	Metres (m)	% of total	Porosity (%)	Permeability (mD)
Wet aeolian sandflat	46.99	61.42	9.23 (9.07)	0.08 (0.05)
Damp aeolian sandflat	9.13	11.93	13.72 (13.46)	1.19 (0.30)
Aeolian sandflat	8.45	11.04	9.35 (9.30)	0.28 (0.08)
Fluvial sheetflood/wadi	6.56	8.57	12.71 (11.56)	1.23 (0.47)
Lake	3.14	4.1	7.20 (7.14)	
Dry aeolian sandflat	1.83	2.39	13.40 (12.42)	8.97 (2.32)
Aeolian dune	1.72	2.25	18.64 (16.70)	33.9. (10.4)

Table 5

Depositional environments of the core with accompanying porosity and permeability. Arithmetic mean with geometric mean within brackets. (Table taken from Nlog.nl)

Aeolian dune and dry aeolian sandflat-sandstones seem to display the highest cement percentages (Nlog.nl). Damp and dry aeolian sandflats and fluvial depositions have lower cement abundances. Anhydrite is mostly determined in the 'dryer' environments. The clays are more found in the 'wetter' settings and less in the 'dry' environments.

The pores are mostly micropores that are associated with clays, compacted and cemented intergranular pores and dissolution pores. Macropores are mostly found in the 'cleaner' samples, but are often secondary dissolution pores. These are intergranular and do not enhance the permeability. The good connected intergranular macropores are only found in the aeolian dune and dry sandflats depositions. This better permeability is also seen in Table 5. The largest part of the core has a rather low permeability.
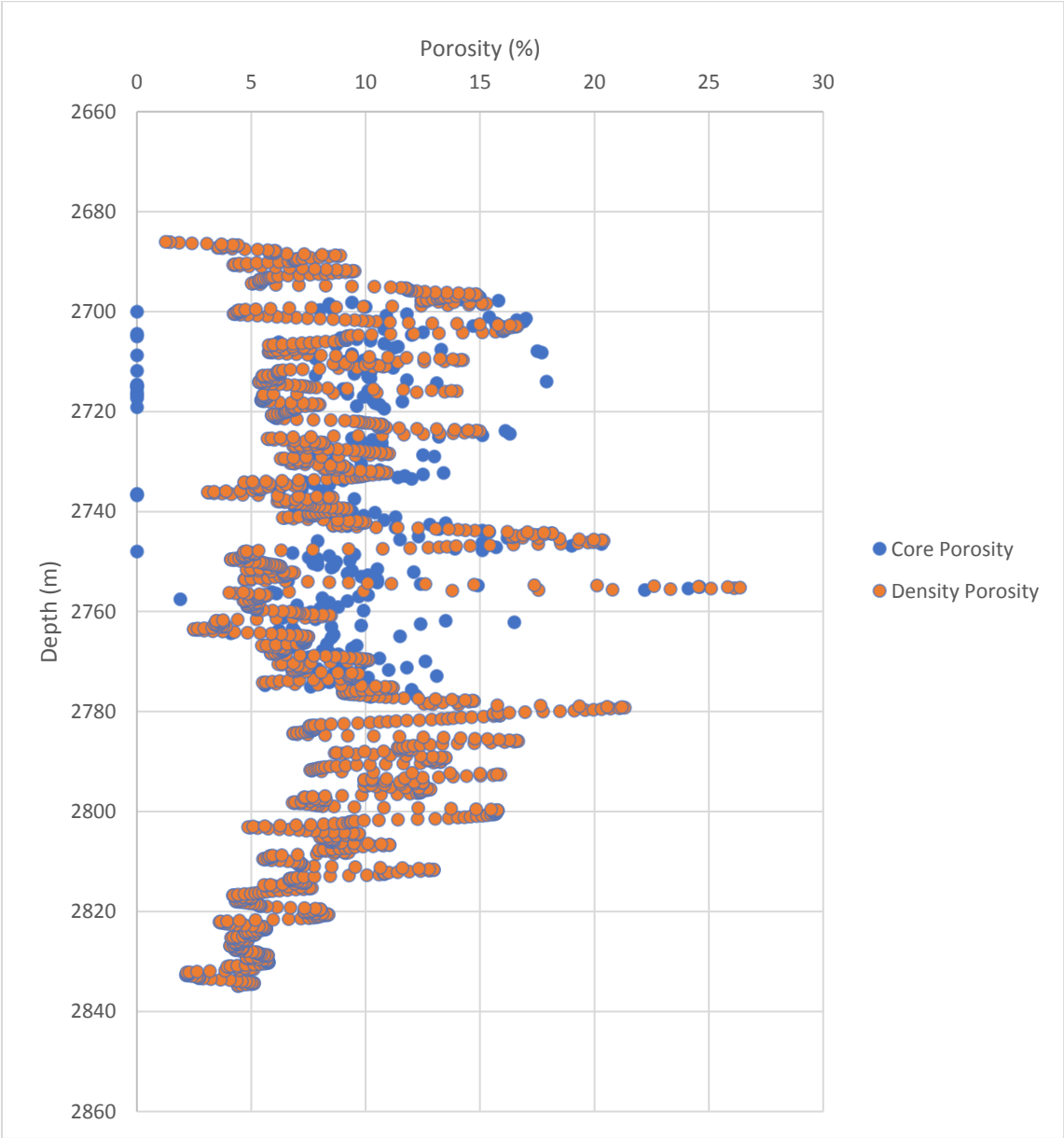

Figure 9 A comparison of the core porosity and porosity based on density measurements from well logging. The core porosity is measured on core plugs. The density porosity is calculated using the density porosity formula. The density used for the fluid in this graph is 1 g/cm³. This density gave the best results. Noticeable is the variety in porosity, both in the core porosity as the density porosity. This would imply streaks of higher and lower porosity, which might indicate permeability streaks.

1. Density porosity from matrix, log and fluid densities.

$$\Phi_{density} = \frac{\rho_{matrix} - \rho_{log}}{\rho_{matrix} - \rho_{fluid}}$$

The above formula is the density porosity formula. The matrix density is taken at 2,65 g/cm^3 as the density for sandstone. Figure 9 is depicting the variation in porosity in the Cranberry field. Both the porosity from core flooding experiments as well as the calculated porosity based on the density show a wide variety in porosities from 1% to 26%, with an average of 10%. In the density porosity a zigzag pattern is discernible. This could indicate the various depositional environments and a certain cyclicity in them.

The caprock exists of the Ten Boer shale and the Zechstein formation. Van der Linden *et al.* (2015) performed mechanical experiments on the Ten Boer shale and determined that it existed of two lithologies: shaly sandstone and shale. The shaly sandstone had a Young's Modulus of 19.9 ± 3.9 GPa and a Poisson's Ratio of 0.09 ± 0.03. The shale had a Young's Modulus of 12.8 ± 1.7GPa and a Poisson's Ratio of 0.04 ± 0.03. Hangx *et al.* (2010) performed mechanical experiments on anhydrite. The Young's Modulus was determined to be 50 GPa, but the experiment was performed with pristine samples, which was thought not to be a representation of nature. It was scaled to 5 GPa. Shale, anhydrite and halite are characterized by low porosity and low permeabilty.

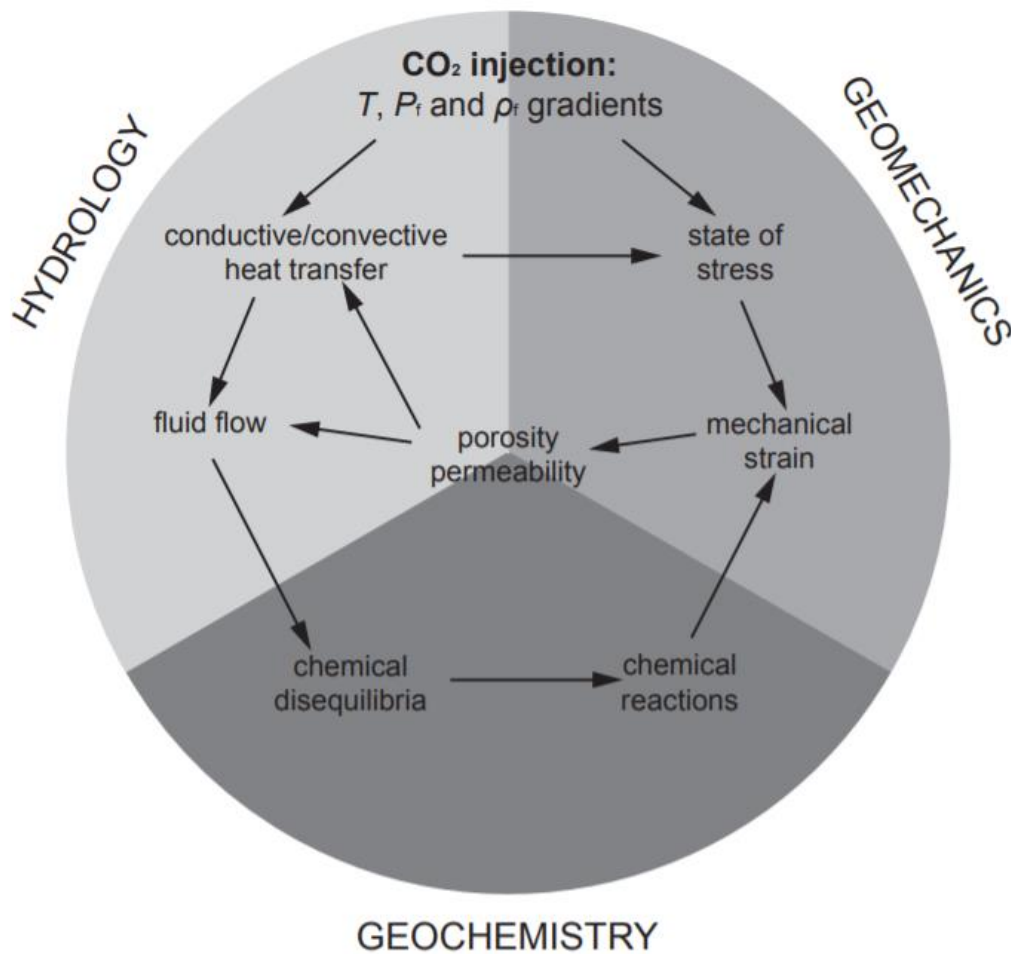# 4. Potential subsurface effects of CO_2 injection and gas production

Figure 10 Interlinkage of subjects relating CO_2 injection from Johnson et al. (2004).

4.1. Introduction

As the effects of CO_2 storage are directly linked to each other, the graph of Johnson *et al.* (2004) (Figure 10) is used as a guide to progress through possible effects in an orderly way. First the chemical effects will be described. Second the mechanical effects are discussed. Third the hydrological effects are touched and fourth the porosity and permeability implications are noted. After the listing of all the possible implications of CO_2 storage and production of natural gas, the effects are assessed in a discussion and grouped in more and less important. Importance is decided on the likelihood of the effect influencing the proposed idea of simultaneous production and injection and the following long term storage. Figure 11 shows a schematic diagram with the zones in which effects are expected.

At the same time the effects of natural gas production are discussed in the same way. Each chapter will have the effects of production described as well.

4.2. Geochemical effects

To determine geochemical effects in any field, the most important information pieces are the characteristics of the field itself. The composition of the brine, dissolved calcium and sulphate, present in the reservoir and/or aquifer is of significant importance for the amount of calcite that can dissolve or the precipitation of minerals (Rosenbauer *et al.*, 2005). The composition of the reservoir rock has in its turn effect on the solubility of the CO_2. As the reservoir rock might have a lot of

carbonate rock content, which dissolves easily, there might be less fluid remaining to dissolve CO_2. The equilibrium of the carbonate dissolution equation will thus have an impact on the equilibrium of the CO_2 dissolution equation. To determine the composition of the reservoir, a core sample would need to be analysed through XRD and thin section analysis. The composition of the brine would need to be determined through a sample taken from the well as well. If one or both are not available, an option would be to look into data from fields in the vicinity of the target field.
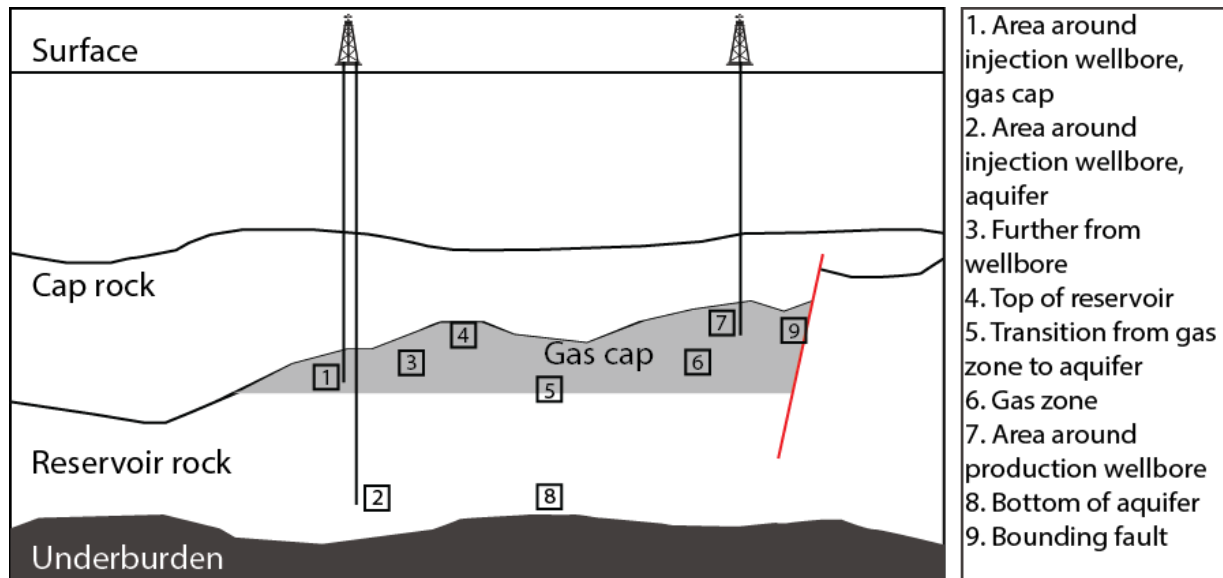

Figure 11 Schematic depiction of a combined production/injection site. The boxes are zones within the project. Zone 1 indicates a one-phase system, near dry, with possible salt precipitation which might induce clogging, but also possible dissolution of minerals. Zone 2 indicates the option of injecting into an aquifer and where CO_2 will dissolve into the brine. Zone 3 is further from the wellbore and indicates possible dissolution of minerals, precipitation of minerals, possible residual trapping and a two-phase system of $scCO_2$ and CO_2 in solution. Zone 4 shows the location where CO_2 might gather as CO_2 possibly floats to the top of the reservoir, a kind of CO_2 rich cap. Zone 4 also demonstrates one of the possible trapping mechanisms, namely a structural trap. Zone 5 marks the dissolution of CO_2 into the brine, which is also a trapping mechanism, namely solubility trapping. Zone 6 is the natural gas zone, which at the start consists of the entire reservoir. Zone 7 specifies the production site, where the pores are emptied, which might induce micro fractures due to a larger effective stress. Zone 8 shows the area where the dissolved CO_2-rich brine might sink to, as it is heavier than regular brine. Zone 9 indicates a trapping mechanism, another structural trap. This time through a fault, which might reactivate of become stronger due to the change in mechanical state of stress and the change in chemical state.

4.2.1. Chemical reactions

When injecting carbon dioxide into a reservoir, full or empty, the chemical situation will change. The CO_2 will dissolve into the fluids present and will make them more acidic (Kaszuba *et al*., 2003). This may lead to a range of chemical reactions, depending on the availability of reactive minerals. Typical reactions include:

2. Dissolution of CO_2 into water (Plummer&Busenberg, 1982)

$$CO_2 + H_2O \leftrightarrow H_2CO_3$$

$$H_2CO_3 \leftrightarrow H^+ + HCO_3^-$$

$$HCO_3^- \leftrightarrow H^+ + CO_3^{2-}$$
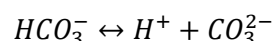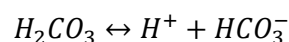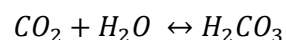
3. Calcite dissolution or formation (Plummer&Busenberg, 1982)

$$Ca^{2+} + CO_3^{2-} \leftrightarrow CaCO_3$$
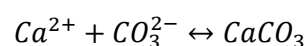
4. Siderite formation from hematite(Palandri *et al.,* 2005). This reaction uses SO_2 as a reducing agent. Organic acids can fulfil this role as well.

$$Fe_2O_3(hematite) + 2CO_2 + SO_2 + H_2O \leftrightarrow 2FeCO_3(siderite) + H_2SO_4$$
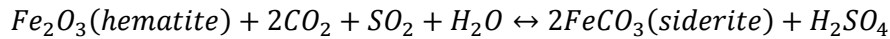
5. Dolomite dissolution or formation (Usdowski, 1968)

$$Mg^{2+} + CaCO_3 \leftrightarrow (CaMgCO_3)_2$$

6. Ankerite dissolution or formation (based on Boles, 1978)

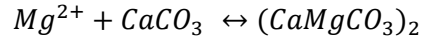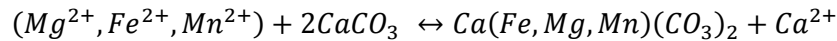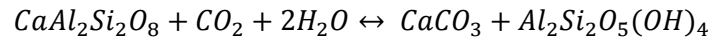$$(Mg^{2+}, Fe^{2+}, Mn^{2+}) + 2CaCO_3 \leftrightarrow Ca(Fe, Mg, Mn)(CO_3)_2 + Ca^{2+}$$

7. Kaolinite/calcite precipitation after anorthite dissolution

$$CaAl_2Si_2O_8 + CO_2 + 2H_2O \leftrightarrow CaCO_3 + Al_2Si_2O_5(OH)_4$$

Next to the above mentioned reactions, an important supplier of cations are clay-minerals. They supply Ca^{2+}, Fe^{2+}, K^+ and Mg^{2+} cations. Though CO_2 dissolution will create only a weak acid, pH=4, (Rohmer *et al.*, 2016) and the buffering of calcite present in a reservoir might even further compensate the acidification, this will not prevent the reservoir fluids from being more acidic. As calcite has a buffering function, it is likely that a part of the calcite that has contact with fluids will dissolve. It is possible that some calcite has a coating (Hangx *et al.,* 2015) which prevents dissolution or that the fluid-rock ratio does not permit that all of the calcite dissolves as there is just not enough fluid for the calcite to dissolve into. Next to CO_2 and calcite, also iron, magnesium and anorthite can react due to the changing environment. ((B)Hangx 2005) Anorthite will dissolve within a more acidic environment and thus making it possible for secondary kaolinite to precipitate, next to calcite. ((A)Hangx (2005)) Magnesium-cations will react with the carbonate-anions and form magnesite (Kaszuba *et al.*, 2003) and iron-cations can react to form siderite ((A)Hangx, 2005). Next to these minerals, quartz can dissolve as well, though not as readily as calcite for example. Quartz will dissolve more easily in more basic conditions, though quartz will dissolve in more acidic conditions as well (Brady&Walther, 1990).
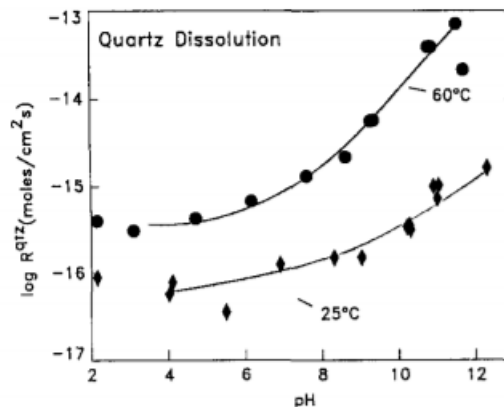
Figure 12 The solubility of quartz with respect to pH. Diamonds represent 25 °C rates, circles represent 60 °C rates. The size of the symbols are indicative of the degree of error in the rates themselves. (Taken from Brady&Walther, 1990)

In the study of Rathnaweera *et al*. (2015), quartz corrosion was observed both in the experiments with brine as in the experiments with water. The study concludes that a silicate-cemented sandstone, which is mostly made up of quartz is thus more suitable for CO_2 storage, because the cement does not dissolve as with carbonate-cemented sandstone. This conclusion was pH independent and the fluid-rock ratio was not taken into account. For the carbonate cement to dissolve, there needs to be

fluid present. For all the carbonate cement to dissolve, there needs to be sufficient fluid present, preferably fluid flow to keep the dissolution reaction going to prevent saturation. In correspondence with Rathnaweera et $al.$ (2015), ((A) Hangx 2005) quartz dissolution is found to be independent of pH in between 2 and 7 and more dependent on temperature. This suggests that any dissolution of quartz already would have taken place before CO_2 injection. This could be visible on thin sections under a microscope. This would mean that the contacts between quartz grains are not point contacts, but line contacts through pressure solution. A process where a mineral can dissolve under pressure and will precipitate under less pressure and thus transfer material from the point contact to a location adjacent to the point contact and thus creating a line contact. Interestingly, Marbler et $al.$ (2013) found secondary carbonate minerals that had precipitated during the experiments on sandstone. (Hangx (2006) and Kaszuba et $al.$, (2005)) The study of Nover et $al.$ (2013) found that in a range of temperatures (100-200°C) and pressures (10-20 MPa) and after experiments with $scCO_2$ the elements Ca, Mg, Al and K were mobilised in two types of sandstones. They found also that clay and feldspar were partially dissolved. As these elements were dissolved in a more acidic environment, the influx of brine with a more neutral pH might induce precipitation of these elements within newly formed minerals (Kaszuba et $al.$, 2005). Brine influx can happen through an underlying aquifer. Abdullah et $al.$ (1999) studied the possible swelling of clays in relation to decreasing pH. An increasing pH was paired with more oriented clay particles. It thus needs to be determined whether clays present in a reservoir are swelling clays like smectite and montmorillonite or non-swelling clays like illite and kaolinite to even suggest the possibility of swelling clays. Horsrud et $al.$ (1998) studied shales of the North Sea and the data suggests that the difficult to distinguish illite/smectite clays are near 100% illite beneath a depth of more than 2000m. Hower et $al.$ (1976) found that between 2000 and 3600 m depth the ratio illite/smectite transitions from 20/80 to 80/20. Jennings&Thomson (1986) observed a transition from a mixed illite/smectite layer to a 100% illite layer in a temperature range from 70-210 °C. Both Hower et $al.$ (1976) and Jennings&Thomson (1986) support Horsrud et $al.$ (1998) in the observation of near 100% illites beneath a depth of 2000m. Next to the dissolution of carbonate cement, anhydrite is also likely to dissolve in more acidic conditions (Hangx et $al.$, 2015). Anhydrite is often a cement as well. Of course, anhydrite and carbonates are also part of sealing formations as well. However due to the low porosity and low permeability of sealing formations, fluids cannot penetrate the seals and thus dissolution is very limited. A low porosity limits the reaction surface and a low permeability limits the amount of fluids present which prevents the reaction, also as the fluid-rock ratio is very low.

An interesting chemical reaction is also the evaporation of salts that were present in the brine, as the fluids are completely saturated with dissolved minerals, salts and CO_2, and dry $scCO_2$ is injected into saline aquifers (André et $al.$, 2007, and Miri et $al.$, 2015). Miri et $al.$ (2015) is even warning that this process could be self-enhancing and thus play a larger role while injecting CO_2 that previously thought. It could be self-enhancing as the produced salts increase the surface area for evaporation. The impact of this process is a decreasing porosity and permeability, which can limit the rate of CO_2 injection and the overall storage capacity of the reservoir.

Research has been done into the effect of chemical reactions on the mineral composition of a reservoir. Hangx et $al.$ (2015) looked into the Werkendam field, a natural CO_2 holding reservoir near Rotterdam, and compared it to a field in the near vicinity which does not have CO_2 in it. They found only minor chemical variations between both the reservoirs. Both Heinemann et $al.$ (2013) and Wilkinson et $al.$ (2009) looked into the Fizzy gas field, an offshore UK gas field, to determine the effect of CO_2 on a reservoir on a geological timescale. Both concluded that the storage capacity in minerals in minimal and structural trapping provides by far the largest amount of trapping. Waldmann et $al.$ (2014) observed that primary mineral content is important to determine potential

reactions as two different mineral assemblages were modelled and showed different mineral reactions.

4.2.2. Chemical disequilibria

All of the above reactions start of due to the fact that injecting CO_2 in a reservoir will create a chemical disequilibrium (Rochelle *et al* 2004). However, it has been mentioned that a reservoir can already be in a disequilibrium at the onset of injection (Baines&Worden, 2001). This could mean that a reservoir won't be reaching a state of equilibrium after injection has ceased, even on a geological timescale. A possible explanation could be the influx of new fluids though an aquifer that communicates with the pore fluids in the gas reservoir above.

The reservoir can also be put into disequilibrium due to the production of natural gas. As the gas is extracted, water from the aquifer beneath might infiltrate, which would exchange gas with brine.

4.3. Mechanical effects

After indicating possible geochemical effects of CO_2 injection, this subsection will focus on the geomechanical effects of CO_2 injection. Similar to the last chapter, to get a clear indication of which of the following might be more or less interesting the state of the reservoir and seal on a mechanical level needs to be clear. The state of stress, which includes overburden, pore fluid pressure, tectonic stresses among others, is of particular interest to determine changes to the state of stress which might occur.

Next to the state of stress, the mechanical strength of the reservoir and cap rock is important information. In an ideal situation this is determined through mechanical experiments, however the availability of material, time and/or funds can limit the carrying out of experiments. In this case an best estimate is needed. This can be achieved through the use of empirical relations relating rock strength to porosity or wave velocity (Chang *et al.*, 2006). Further explanation can be found in the subsection 'Failure Criterion'. In this section the processes and parameters that influence the strength of the rock are discussed.

Marbler *et al.* (2013) tested both silicate and carbonate sandstones with H_2O saturation with H_2O as pore fluid or CO_2 as pore fluid. The silicate sandstones had a slightly higher uniaxial compressive strength with CO_2 after the experiments than the carbonate sandstones. The paper also couples rock strength to saturation degree, confining pressure, pore fluid pressure and temperature. The main reason for decreasing rock strength was determined to be dissolution of minerals. This, together with chemical alteration, also weakened the grain structure and thus elastic properties.

Rathnaweera *et al.* (2015) tested silicate sandstone in a dry, water saturated and brine saturated environment before and after $scCO_2$ injection. In a dry environment the strength decrease was 13%, which indicates that even injecting in a part of the reservoir with almost no pore fluid, the strength of the rock is affected. Marbler *et al.* (2013) also concluded a strength reduction in a dry environment. In the water saturated environment the strength reduction was 46% (Rathnaweera *et al.*, 2015). The loss of strength is believed to be coupled to chemical changes to the rock. In the brine saturated environment, the salinity is of interest as well. The paper of Rathnaweera *et al.* (2015) concluded that in the experiments with 10%, 20% and 30% NaCl, the strength of the rock was higher when CO_2 was injected than without CO_2 injection. This rock had only 4% calcite, which limits the effects of calcite dissolution on rock strength. The conclusion that a higher salinity decreases the weakening effect of CO_2 injection is based on the higher saturation level of the present fluids. The CO_2 has a limited opportunity to dissolve into the fluid, which limits the acidification. Rathnaweera *et al.* (2015) also indicated that the salinity increases with depth and that the dissolution of CO_2 is reduced with higher

salinity. Lastly, an interesting find is that the samples injected with $scCO_2$ were failing in a 'splitting' type, whereas the 'normal' samples failed in a 'shearing' type.

Hangx *et al*. (2013) tested poorly consolidated carbonate and quartz cemented sandstones. The calcite dissolved completely, but the rock strength was not influenced. The paper concludes that the quartz was the main consolidator of the rock, which did not dissolve, and thus the strength was not influenced. Nover *et al*. (2013) also concluded from extensive experiments that treatment with $scCO_2$ did not influence the uniaxial compressive strength of the sandstone samples enough to fall outside the range of strengths attributed to sandstones. Hangx *et al.* (2015) conducted research on the Werkendam natural CO_2 field and its non-CO_2 containing brother. The long-term exposure to CO_2 did not change the mineral assemblage exceedingly, however this was partly caused by a bitumen coating on some minerals. In some small zones a considerable amount of anhydrite cement was dissolved, which did decrease the rock strength in those zones as the porosity was increased. Busch *et al.* (2014) studied the Navajo sandstone, which is a natural CO_2 reservoir and compared the sandstone to results from reactive transport modelling. The differences of samples that had reacted with CO_2 and samples that hadn't reacted was associated with geological history rather than the effects of chemical reactions with CO_2. Next to this explanation of differences, the impact on the mechanical strength was found to be low.

4.3.1. State of stress

The state of stress of a reservoir is often a long term condition which is changed due to the production of natural gas and in this case the injection of CO_2. On the production side of the reservoir the pore fluid pressure is reduced and thus the effective stress (Effective stress = lithostatic pressure – pore pressure) becomes larger. On the injection side of the reservoir it is the exact other way around. And doing both simultaneously increases the difference in stress state between the production and injection side even more. As both the changes in state of stress of production (Segall&Fitzgerald, 1998 and Van Eijs *et al*, 2006) and injection (i.e. Mathias *et al*., 2009(A) and Mathias *et al*., 2011) separately have been modelled, it is necessary for this idea to model them together to research the change in in state of stress quantitively. Mathias *et al*. (2009(B)) provides a methodology for the injection type of modelling.

This change in state of stress will move the Mohr-Coulomb circle closer (injection) and further away (production) from the failure envelope. Especially at the injection site, it is of interest to see how much the effective stress is changed and to thoroughly analyse the possibility of failure. Hangx *et al*. (2015) looked into this change of state of stress and concluded that failure is unlikely in the researched reservoir. That reservoir had local nodules of anhydrite dissolved in the CO_2 rich part, which affected the rock strength very locally. However the grains were protected by a bitumen coating, thus the results on the mechanical strength of a reservoir cannot be extrapolated without thought to possible locations for this project. Another conclusion worth mentioning from this paper is that the spread of the dissolving material is of interest for the rock strength.

4.3.2. Mechanical strain

Rohmer *et al*. (2016) published a large review on possible effects of CO_2 injection. It mentioned time-dependent mechanical behaviour being affected by CO_2 injection due to the dissolution of minerals. As the reservoir is producing on one side, subsidence is of interest to look into on that side of the reservoir. Naturally breakthrough of CO_2 will tried to be avoided as long as possible, however when breakthrough will occur, the CO_2 might induce dissolving of minerals, thus decreasing the strength of the reservoir on a location where the pores already are more empty and more in danger of collapsing, or at least where the grains are under more stress. As subsidence is a possibility on the production side of the reservoir, on the injection side there is a possibility of bulging, because initially

the project is injecting in a full reservoir and thus increasing the pore pressure. Both subsidence and bulging might have impact on the porosity and permeability of the reservoir as well as mechanical strain can change pore shape and influence permeability and thus fluid flow. As both can induce the so called flexural bending of a reservoir, a model might be made where both processes are happening simultaneously and thus might induce a sinusoidal shape of the caprock. Of interest as well is whether or not the induced strain is recoverable or not. More on flexural bending in the subsection 'Flexural Bending'.

Liteanu&Spiers (2009) looked into the effect of pore fluids with varying salinity and saturated with CO_2 on porous carbonates. This might be similar to a carbonatic cap rock. The results showed that a low salinity reduced compaction creep, whereas a high salinity increased the compaction creep compared to the non-CO_2 saturated samples.

Hangx *et al.* (2010) performed uniaxial experiments on quartz sand and feldspar sand aggregates. They reached a couple of conclusions. Compaction occurred in two phases: an instantaneous phase and a creep phase. Experiments performed at room temperature on the quartz samples showed that both types of compaction increase with increasing pH of the aqueous fluid. The time-dependant creep rate decreased after injecting CO_2 under high pressure into the sample. In both phases of compaction the mechanisms of deformation were microcracking and grain rearrangement. As for pressure solution as a creep mechanism, or other dissolution processes, there was no sign of such a process and it was expected that the rate would be too slow to play a role in these experiments. As injection of CO_2 decreases the pH of a fluid, it is expected that negative mechanical effects will be minimal, according to this paper.

Cerasi *et al.* (2017) performed uniaxial experiments on shale to determine if the shale can close potential fractures with creep deformation. The sample exposed to acidic fluid had a higher creep rate than the sample which was exposed to a neutral fluid. The sample exposed to scCO2 showed a higher creep rate than the sample exposed to neutral fluid as well and indicates that under higher pore pressure creep deformation can still occur. The experiments were conducted on Pierre shale.

4.4. Hydrology
The third area of potential effects of CO_2 injection is hydrological. Points of interest within this area are fluid flow and heat transfer.

4.4.1. Fluid flow
André *et al*. (2007) stated that dissolution of all the injected CO_2 in an aquifer may take several thousands of years. Of course the dissolution process is fast and at first dissolution and injection will keep up, but the amounts of CO_2 that need to dissolve will take a long time. The CO_2 can travel through the aquifer and as mentioned in the geochemical part, minerals can dissolve and precipitate. This will influence the permeability and thus the fluid flow in an aquifer. Their modelling results of injecting scCO$_2$ are stating that around the well there is a one-phase system of scCO$_2$, further away there is a two-phase system of scCO$_2$ and CO_2 in solution. (Location 1 and 3 on Figure 11)
Fuller *et al*. (2006) modelled a three-phased situation for sequestration of CO_2 in a saline aquifer. They found that injecting dry scCO$_2$ will cause the water in the brine to evaporate, increasing the salinity of the brine, which in turn will eventually lead to precipitation of the salts within the brine.
Giorgis *et al*. (2007) investigated the formation of halite around an injection well. They came up with similar results of salt precipitation. However they found that the extent is dependent on the movability of the brine. Low movability limited to extent of salt precipitation, while in the other case the extent went further. Especially in the second situation the effect on the permeability of the aquifer might be of concern.
Pruess &Muller (2009) investigated how some of these effects of CO_2 injection could be limited. They suggest injecting a slug of fresh water prior to injection. Possible effects that can be mitigated that

way are salt precipitation by formation dry out and thus reducing the permeability and flow through the reservoir. Hurter *et al.* (2007) ran several models with a compositional simulator and highlighted the need for studying the effects before injection commences to determine the best injection strategy. These experiments were done with an aquifer environment. It is likely that injection in a saline aquifer, with enough fluids to sustain dissolution reactions and possible salt precipitation, will be different from injection into a depleted gas reservoir, where fluid is more scarce. Kleinitz *et al.* (2003) investigated salt precipitation in a gas reservoir from reservoir water. Again salt precipitation reduced the permeability and injecting fresh water is found to be a workable solution.

Aside from solubility trapping, the trapping of CO_2 because of its dissolution into reservoir fluids, which makes the fluid denser and then sinks to the bottom of the reservoir and thus prevents leakage through the caprock (Location 8 on Figure 11), another form is capillary trapping. CO_2 can be trapped by it being in the gas phase and not being able to overcome the capillary forces needed to dissolve into the not yet fully saturated fluids (Ulker, 2009). However, CO_2 will be in the super critical phase for most potential storage locations and that potentially changes the capillary entry pressure that is needed. Alkan *et al.* (2010) investigated the interplay between salinity, capillary pressure, dissolution and drying-out. They looked at how those parameters could influence the potential storage capacity of an aquifer for CO_2. Capillary forces have a great influence, because large capillary forces would force the injection pressure up and to reduce the gravitational segregation of CO_2 gas above, then CH_4, Brine with CH_4 and then brine with CO_2. Bachu&Bennion (2008) interpreted that pressure, temperature, salinity and pore size distribution are key factors to determine capillary pressure, interfacial tension, permeability and other transport related parameters. Capillary trapping might also happen to the methane if the reservoir being depleted.

4.4.2. Conductive/convective heat transfer

The most important effect in heat transfer is the Joule-Thomson cooling effect. This effect impacts injecting CO_2 in a depleted reservoir. The injected CO_2 expands quickly after leaving the well into the reservoir. The expansion follows from a pressure drop from being in the well to being in the depleted reservoir. This expansion reduces the pressure on the atoms as they have more space and the temperature will drop. This rapid cooling might induce the growth of hydrates, freezing of pore fluid, or induce thermal fracturing, a rapid cooling of the rock which causes shrinkage and can induce micro cracks.

Oldenburg (2007) investigated the impact of this effect. For smaller (<10bar) pressure drops, the effect is minimal, for a large pressure drop (>50bar) the temperature would decrease with 20°C, which would be a significant drop in temperature and likely would cause problems. However the 50 bar drop was a theoretical example case and would not occur in practice. Oldenburg (2007) stated that the rate of injection depends on the formation injectivity and would normally be in the range of 5-10 bars (0.5-1.0 MPa) for a high grade gas reservoir. Also he concluded that lower permeability increased the Joule-Thomson effect.

Figure 13 Joule-Thomson coefficient for CO_2 as a function of pressure and temperature. (Data from NIST Webbook, figure taken from André et al. (2010))
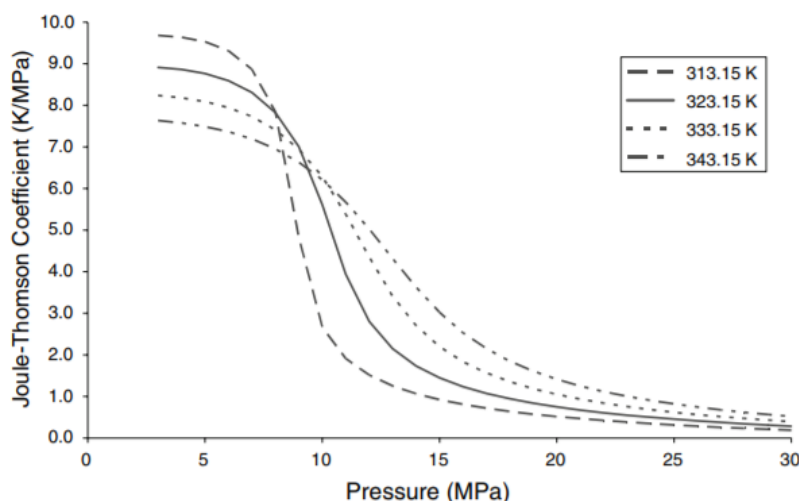
Li *et al.* (2014) noticed the possibility for the effect in an aquifer at the Ordos CCS project, when a temperature drop of 5°C was noticed at the depth of the aquifer. Bielinski *et*

al. (2008) and André *et al.* (2010) both performed modelling of CO_2 injection into a saline aquifer. André *et al.* (2010) modelled a carbonatic aquifer and its chemical reactivity to $scCO_2$ injection. They observed a maximum temperature variation of 3°C, which has little to no effect on the reservoir behaviour.

André *et al.* (2010) used the following standard formula for the Joule-Thomson effect.

8. $\mu_{JT} \approx \dfrac{\Delta T}{\Delta P}$

With Figure 13 the Joule-Thomson coefficient can be determined for a certain environment, which then can be used in the formula to calculate the temperature drop for a certain pressure drop.

Bielinski *et al.* (2008) modelled CO_2 injection to determine the possibility to use temperature measurements to determine the propagation of CO_2 in the reservoir. They looked into non-isothermal effects and the Joule-Thomson effect is one of those effects. They did observe the effect, but it only lowered the temperature by a few degrees, which was not significant enough to use for monitoring. However other non-isothermal effects proved significant enough to use temperature as an effective monitoring parameter.

Gor&Prévost (2013) modelled CO_2 injection into the Krechba aquifer during a 10 year period with varying injection temperatures. They showed that an injection temperature of 40-50 °C would result in tensile stresses in the caprock near the injection well, which resulted in fractures. If the CO_2 would be injected with the same temperature as the aquifer, the stresses would remain compressive. Next to the formation of fractures due to tensile stresses, the increased pressure in the reservoir would encourage the propagation of the fractures in the caprock.

4.5. Porosity and Permeability

The effect of injection of CO_2 on the porosity and permeability of a reservoir has been hinted and discussed in the chapter before. The geochemical, geomechanical and hydrological effects cannot be discussed without mentioning porosity and permeability as well. This chapter will thus be a short recap.

Nover *et al.* (2013) concluded that the effect of $scCO_2$ is not very large. The porosity increased less than 2vol% and the permeability increase was 1.5 times the permeability measured before the experiment. However Rimmelé *et al.* (2010) concluded that the sandstone, when exposed to wet $scCO_2$, had a permeability that had increased 7 to 10 times. The porosity increased 2-6%.

As mentioned before precipitation of salts and minerals can decrease the porosity and permeability, however the dissolution of minerals can increase both the porosity and permeability. Hangx *et al.* (2015) found that in a long term exposed reservoir, the zones which were not protected with a bitumen coating had a larger porosity. This would suggest that the dissolution would be the prevailing process. Mechanical strain can have an influence on porosity and permeability as well and thus on fluid flow as well.

5. Assessment of effects for the Cranberry Opportunity

For the assessment the same order will be used as in the previous chapters.

5.1.1. Discussion Chemical effects

The example project Cranberry Opportunity is anhydrite cemented and has a rather low and heterogeneous porosity, 1.9 – 24.6% with an average of 10.44%. It does hold feldspars and a high fraction of clays. It has been described as a shaly sandstone. The porosity will be later discussed in depth, but for the chemical situation in the reservoir it is important. The key word in this being fluid-rock ratio. If a reservoir has low porosity, the amount of fluid present in the rock will be lower as well and usually reduces the rate of reactions (Huang *et al.*, 1986). This will also reduce the amount of fluids where CO_2 can dissolve into and other minerals as well, thus reaching saturation quicker. The

low porosity also reduces the reaction surface of the fluids with the minerals. This might slow down reactions and even, if some reactive minerals are not connected to a pore, prevent reactions.

As a preliminary analysis of the potential chemical effects of CO_2 injection into a reservoir, chapter 4.2 gives a starting point to look into potential reservoirs. Areas of interest are mineral content and fluid-rock ratios. Minerals that are important to notice are for example anhydrite, feldspars and calcite. The Cranberry field has a very low to no amount of calcite. Hangx *et al*. (2015), Heinemann *et al*. (2013) and Wilkinson *et al*. (2009) observed minimal changes in the chemical composition of the reservoir with CO_2 in the picture. However, enough research is directed at potential dissolution of calcite, anhydrite, feldspars and other minerals to not take 'minimal chemical change' at face value. When the composition of the reservoir is known, along with other characteristics such as porosity and permeability, extensive reactive transport modelling is advised to analyse potential reactions and associated effects on the reservoir. When considering reactive transport modelling, characteristics of interest might be mineral surface area as this impacts the possible reactivity (Waldmann *et al*., 2014) and the residence time of the CO_2 saturated brine as chemical reactions take time. Reactive transport modelling might be best focused at the so called permeability streaks with higher permeability and porosity, as that is where the CO_2 will reside mostly as well as that is the location of possible higher fluid content.

As for the reactions occurring in the reservoir, the expectation is that the anhydrite cement is likely to react and dissolve to some degree. The dissolution of feldspars is slow, but dissolution will most likely occur during injection. But as mentioned in the works of Hangx *et al*. (2015), Heinemann *et al*. (2013) and Wilkinson *et al*. (2009), the chemical changes to the reservoirs they studied were minimal and as each reservoir has an unique chemical composition, reactive transport modelling is needed to determine if anhydrite and feldspars will indeed react.

5.1.2. Discussion Mechanical effects

As mentioned in the Mechanical effects section (4.3), the strength of a rock can be influenced by injection of CO_2, though not in every situation. Mechanical effects are more noticeable short term than chemical effects, though they also work long term. It is of interest to look into the maximum allowed reduction in strength before a rock begins to fail to analyse the safety of CO_2 injection. This needs to be done in combination with the possible changes in the state of stress of a reservoir. The state of stress of a reservoir will influence the possibility of failure as well as the reduction of effective stress by increasing the pore pressure. Reduction of effective stress might cause existing microfractures to reactivate or even reactivation of the faults bounding the field. This specific effect is however difficult to investigate as faults in the subsurface have unknown properties and strengths. The example reservoir Cranberry Opportunity is a unique case as injection and production will be done simultaneously and right from the onset of production. This results in a duality in the change of stress as normally either production or injection occurs to the extent that is planned for this project. The strain that occurs in a reservoir after a period of gas production is likely to be lessened due to the mitigation of the effects due to injection. Another mitigating aspect to reduce the impact of compaction and subsidence is the size of the field. The Groningen gas field, that has yielded problems due to compaction, is humongous in comparison to any other gas field. As the compaction is expected to be minimal, the chance that microfractures will develop at the bottom of the caprock is less than for regular production projects. The big unknown is how the reservoir and caprock will react to the injection in the beginning as the reservoir is still full at that time. At a certain time this will be again of less interest as the pressure in the reservoir is sufficiently diffused. The determination of this time or at least an approximation might be of interest for reservoir modellers. Until such a time,

interest should go to the speed of injection and the associated pore pressure increase. Further discussion on flexural bending in the relevant subsection.

5.1.3. Discussion Hydrological effects

The Joule-Thomson cooling effect will not affect this project as the plan for this project is to inject in a full reservoir and the effect is induced in a depleted reservoir. As for the trapping of CO_2 in an aquifer, that depends on the situation at the project location. At the Cranberry opportunity a study has to be made whether or not the aquifer is an open system or closed system, as in a closed system the pressure might go up, which might result in unwanted effects. As for precipitation of salts, this is always a point of interest. Residual fluids in the gas reservoir or in the brine in the aquifer can both dry out due to injecting dry $scCO_2$, so in both cases the salts within the fluids can precipitate. In a very heterogeneous field with respect to permeability and porosity, this might give problems with injecting $scCO_2$ in time. Capillary trapping is not an issue for the Cranberry Opportunity as the CO_2 will not be in the gas phase, but in the super critical phase.

5.1.4. Discussion effects on porosity and permeability

For this project and other injection projects, this dual effects needs an in depth analysis. The expectation is that the porosity and permeability will both increase as seen in the Werkendam field (Hangx *et al.*, 2015), but to what extent this will occur depends on the reservoir composition. For Cranberry the effect of the factors that will decrease the porosity and permeability (precipitation of minerals) will be possibly be diminished, because one of the plans involves the production of electricity be coupled to a wind farm. The idea is that Cranberry electricity will supplement the production of the wind farm on days where the total capacity of the farm is not reached. On days where the wind farm reaches pull capacity, Cranberry can and will be paused, which offers options for flushing the potential clogged pores. This will decrease the risk of problems with reduced permeability. However if the plans for Cranberry change and injecting a slug of fresh water regularly is not an option anymore, clogging might have an impact on the injection strategy. Cranberry is a very heterogeneous reservoir where the porosity and permeability are on average quite low. The increase of both will not induce major structural problems.

Potential effect	Expected to **not** play a role	Possibly plays a role	Expected to play a role	Further research recommended	Comments
Acidification of pore fluids			*		Pore fluid needs to be present
Dissolution of framework minerals			*	Yes	Extent depends on amount of pore fluid
Dissolution of cement (Anhydrite, calcite)			*	Yes	Extent depends on amount of pore fluid
Chemo-mechanical weakening of reservoir rock			*	Yes	
Precipitation of secondary minerals		*			
Salt precipitation		*			Pore fluid needs to be present
Clogging of pores		*		Yes	Pore fluid needs to be present
Chemo-mechanical weakening of cap rock	*				
Change state of stress			*	Yes	
(Re)Activating faults		*			
Onset of creep			*	Yes	
Reservoir compaction	*				
Flexural bending cap rock	*				
Fractures in the reservoir and caprock	*				
Joule-Thomson cooling	*				
Permeability increase of cap rock	*				

Table 6 Compact list of effects with expected effects.

6. Detailed assessment of geomechanical effects

Earlier the effects of CO_2 storage are listed and discussed for importance. Possible research methods are discussed as well. As it is not within the reach of this project to investigate all the important, or even less important, effects, two effects which are expected to have an impact are further investigated in the following section. First the strength of the reservoir and cap rock is looked into, using the Mohr-Coulomb failure criterion and the work of Freyburg (1972), McNally (1987), Fjaer et al. (1992), Moos *et al.* (1999), Bradford *et al.* (1998), Vernik *et al.* (1993) and the compiling work of Chang *et al.* (2006) (Table 7). This will give an insight into what kind of stress changes the rock of interest can sustain without failing. For the production side the stress changes are well researched, however for the injection side of the reservoir the stress changes are not as well known, especially when increasing the pore pressure from the steady state. Next the elasticity of the cap rock is investigated with the work done on flexural bending. Flexural bending is of interest to give an idea of potential subsidence at the surface and to see what kind of stress can occur during bending, which in turn might induce a failing rock.

6.1. Failure Criterion

A failure criterion is used to determine the strength of a rock. It demonstrates the stress at which causes the rock to break, or fail. Any stress lower than the calculated failing stress the rock should be able to withstand. There are numerous failure criteria available. A selection is listed in Duveau *et al.* (1998). Here the linear failure criterion of Mohr-Coulomb will be used.

The Mohr-Coulomb failure criterion is used to construct a failure envelope (Figure 14), using the formula (19) $\tau = c + \mu\sigma_n \ where \ \mu = tan\phi$. It uses the normal stress σ_n, the friction coefficient μ, which is based on the angle of internal friction ϕ and the cohesive strength c. An analysis can then be made, with an appropriate stress state of σ_1 and σ_3, of the likelihood of a rock to fail or not with the construction of a Mohr circle. The Mohr circle indicates the state of stress. A rock will fail when the Mohr circle hits the failure envelope.
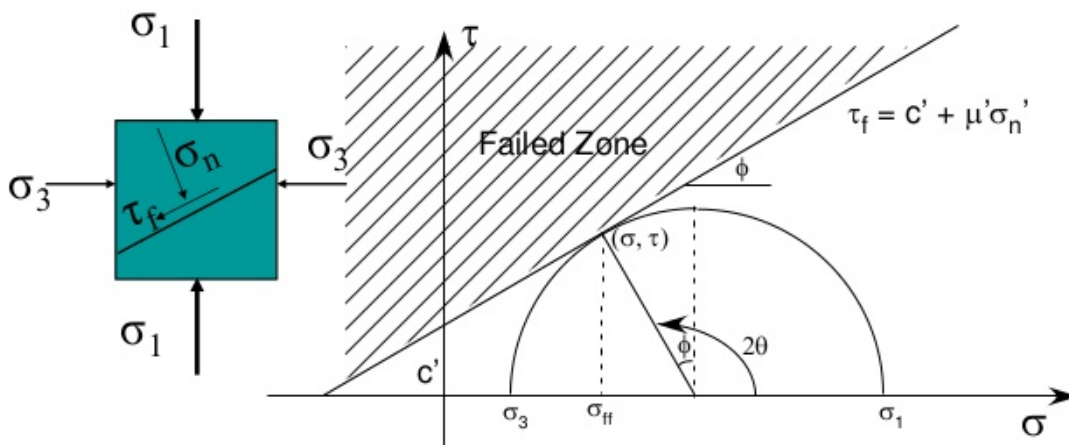

Figure 14 A sketch of the Mohr-Coulomb failure envelope with the failure criterion. (Ullah, 2015)

Ideal input for a failure criterion would be mechanical experiments with core samples from the reservoir in question to determine the cohesive strenght. However, these are not always available. To make a more educated estimate of the strength of the reservoir and cap rock, it is possible to use similar rock types which have undergone mechanical testing (Chang *et al.,* 2006). The paper of Chang *et al.* (2006) accumulates multiple experimental results and possible empirical fits (Table 7). They use different rock parameters to produce an Unconfined Compressive Strength (UCS), which can be turned into the cohesive strength of a rock (S_0 or c) via UCS=$0.5S_0$. (Jaeger *et al.* (2009)

Eq. no.	UCS (MPa)	Origin	Comments	Reference
8	$0.035 V_p - 31.5$	Thuringia, Germany	-	Freyburg (1972)
9	$1200 exp(-0.036 \Delta t)$	Bowen Basin, Australia	Fine grained, both consolidated and unconsolidated sandstones with all porosity range	McNally (1987)
10	$1.4138 x 10^7 \Delta t^{-3}$	Gulf Coast	Weak and unconsolidated sandstones	
11 (4)	$3.3 x 10^{-20} \rho^2 V_p^4 \left[\dfrac{(1+v)}{(1-v)}\right]^2$ $(1-2v) [1 + 0.78 V_{clay}]$	Gulf Coast	Sandstones with UCS>30 MPa	Fjaer *et al.* (1992)
12	$1.745 x 10^{-9} \rho V_p^2 - 21$	Cook Inlet, Alaska	Coarse grained sandstones and conglomerates	Moos *et al.* (1999)
13	$42.1 exp(1.9 x 10^{-11} \rho V_p^2)$	Australia	Consolidated sandstones with 0.05<ϕ<0.12 and UCS>80 MPa	
14	$3.87 exp(1.14 x 10^{-10} \rho V_p^2)$	Gulf of Mexico	-	
15 (8)	$46.2 exp(0.027 E)$	-	-	
16	$2.28 + 4.1089 E$	Worldwide	-	Bradford *et al.* (1998)
17	$254(1 - 2.7\varphi)^2$	Sedimentary basins, worldwide	Very clean, well-consolidated sandstones with ϕ<0.3	Vernik *et al.* (1993)
18	$277 exp(-10\varphi)$	-	Sandstones with 2<UCS<360 MPa and 0.002<ϕ<0.33	

Table 7 Empirical relationships between unconfined compressive strength (UCS) and other physical properties in sandstone. If no reference is given, the formula is unpublished. (Table taken from Chang et al., 2006)

6.1.1. Method

In order to use the paper of Chang *et al.* (2006) and its formulas listed in Table 7, the parameters P-wave velocity (V_p, via Δt), interval transit time (Δt), density (ρ), Young's Modulus (E), porosity fraction (ϕ), Poisson's ratio (v) and the volume of clay fraction (V_{clay}), used in these formulas need to be deduced from well logs and taken from literature research on similar rocks. Δt, as mentioned, is interval transit time, which indicates the ability to transmit seismic waves of the formation rock. It is determined through sonic logging. Δt needs to be in µs/m and can then be used to determine V_p through $V_p = 10^6 / \Delta t$. The Young's Modulus measures the stiffness of a material. It relates stress and strain. The Young's Modulus is taken from Hangx *et al.* (2013) as the material from that study was a brine saturated carbonate cemented sandstone. The Young's Modulus is 15.9 GPa. The strength of that particular sandstone after CO_2-saturated brine flow through was 18.4 GPa. A more fitting rock would be a dry sandstone as the one from Hangx *et al.* (2015), which had a Young's Modulus of 28.2 GPa. However the lowest Young's Modulus is chosen to be on the safe side of the calculation. Poisson's ratio is a ratio between transverse strain and axial strain, so how much a material will be thinning when stretched. The Poisson's ratio is taken from Hangx *et al.* (2015) and is 0.3, which

indicates carbonate rocks. A sandstone would have a Poisson's ratio of around 0.2. A shale would have a Poisson's ratio of over 0.3. The ratio from Hangx *et al.* (2015) is chosen to be on the safe side.

Careful calibration of the raw data of the well logs is needed to yield the input. One of the most important steps is to determine the depth of the rock and how that translates to the raw data from the logs. The logs often shift a couple of meters with respect to the true vertical depth and are sometimes presented in 'depth along hole'. The depth also shifts because of the different starting points for measuring, such as 'rotary table' or 'mean sea level'. To get a correct interpretation, all available logs need to be calibrated to each other in terms of depth. Another step is to determine the fraction of shale in the sandstone. Most raw data is automatically interpreted by software. This interpretation is based on a pure sandstone. If the reservoir rock has a large fraction of shale, the automatic interpretations might give a distorted image of the reservoir. It is thus important to know the fraction of shale and use it in your interpretations. This effect is caused by the incorporation of water into the shale structure, which is interpreted as porosity, but isn't. Measuring devices used in bore holes often use the water content for measuring different parameters such as travel time and porosity, which is distorting in shaly rocks as the water is included in the mineral structure. Comparing the porosity determined while logging with the porosity determined through an experiment performed on a core, is a way to check the log results. During this step, depth calibration is very important as one often compares different data sets. Often the raw logging data produced by the measuring devices, such as density and interval transit time, also needs to be converted into SI units.

After processing the input, the formulas listed in Table 7 are used to calculate an UCS. These will then have to be evaluated as well, because some of the formulas will be based on different types of rock and will yield unrealistic results. An example would be an empirical fit based on an unconsolidated sandstone. It might look as an acceptable result, however the type of rock the empirical fit was based on is so unlike the reservoir sandstone at depth, it should not be taken into account. Ideal would be knowing the UCS of a similar rock in the area as an indicator. Unrealistic results, such as a UCS of below 1, should not be taken into consideration, as they will deviate too much from the actual situation. The remaining results will give a range of UCSs (Figure 15), which after conversion into S_0 can be used to calculate a range of failure envelopes, using $\tau_f = C + \sigma_f tan\phi$. An estimate of the present stresses, like the overburden or vertical stress, will then provide input to construct a Mohr circle. The world stress map (http://www.world-stress-map.org/) can give input into the tectonic regime present at the location of interest, though it can give an 'unknown' tectonic regime as well for locations. For the Cranberry Opportunity it presents an 'unknown'. Looking at close by tectonic regimes doesn't help as both compressive and extensional are found. The stress state calculation from the overburden stress into the horizontal stress is different for an extensional, compressional or hydrostatic regime. Hypothetical calculations for stress are taken from Rutqvist *et al.* (2008).

1. Hydrostatic, where $\sigma_v = \sigma_1 = \sigma_2 = \sigma_3$,

2. Compressive, where $\sigma_v = \sigma_3$ and $\sigma_1 = \sigma_2 = 1.5 \sigma_3$,

3. Extensional, where $\sigma_v = \sigma_1$ and $\sigma_3 = \sigma_2 = \frac{2}{3} \sigma_1$, taking compressive stresses as positive.

Ideal would be to know the exact stress state in the location of interest, however that information isn't always available. At the moment the stress state and tectonic regime is unknown for the Cranberry Opportunity. The hypothetical formulas from Rutqvist *et al.* (2008) are thus used with the overburden as vertical stress. As it is known that the reservoir is overpressured, the hydrostatic tectonic regime is not used in this calculation. As mentioned in Field Specifics, the overburden is 61 MPa.

6.1.2. Results

As the input was calibrated from logging and taken from other sources, the formulas from Table 7 were used to get the results as shown in Figure 15. Formulas 9, 10 and 11 rendered such a small UCS that the bars don't show on the chart. As they are so small, they will be not be taken into account for further analyses and calculations. The same thing goes for formula 5, as it renders a negative UCS. Formula 11 will be used, however note that an UCS between 1-25 is determined to be a very weak rock (Deere&Milller, 1966) and that this will likely not be the case for a reservoir sandstone.
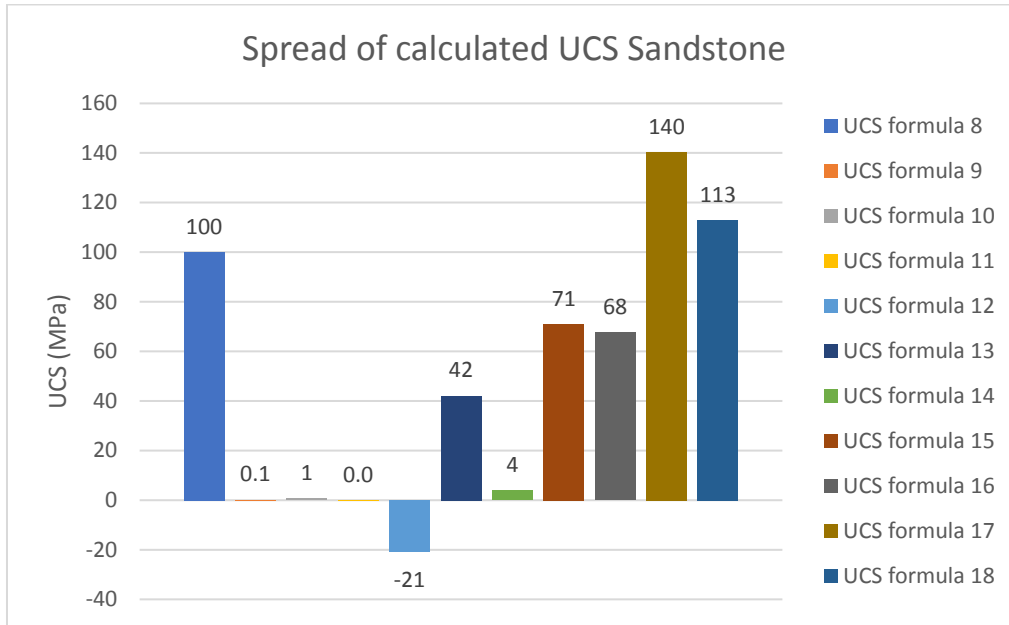
Figure 15 Spread of UCSs, calculated with the formulas listed in table 2.

Using the results from Figure 15 and the hypothetical formulas from Rutqvist *et al*. (2008), Figure 16 was generated. The two failure envelopes for the reservoir were chosen to depict the maximum range of strengths as these were the highest and lowest constructed that were found to be possibly realistic. The two circles depict the compressional and extensional tectonic regime. The calculations can be found in the accompanying Excel sheet which features the formulas and standardized calculations.
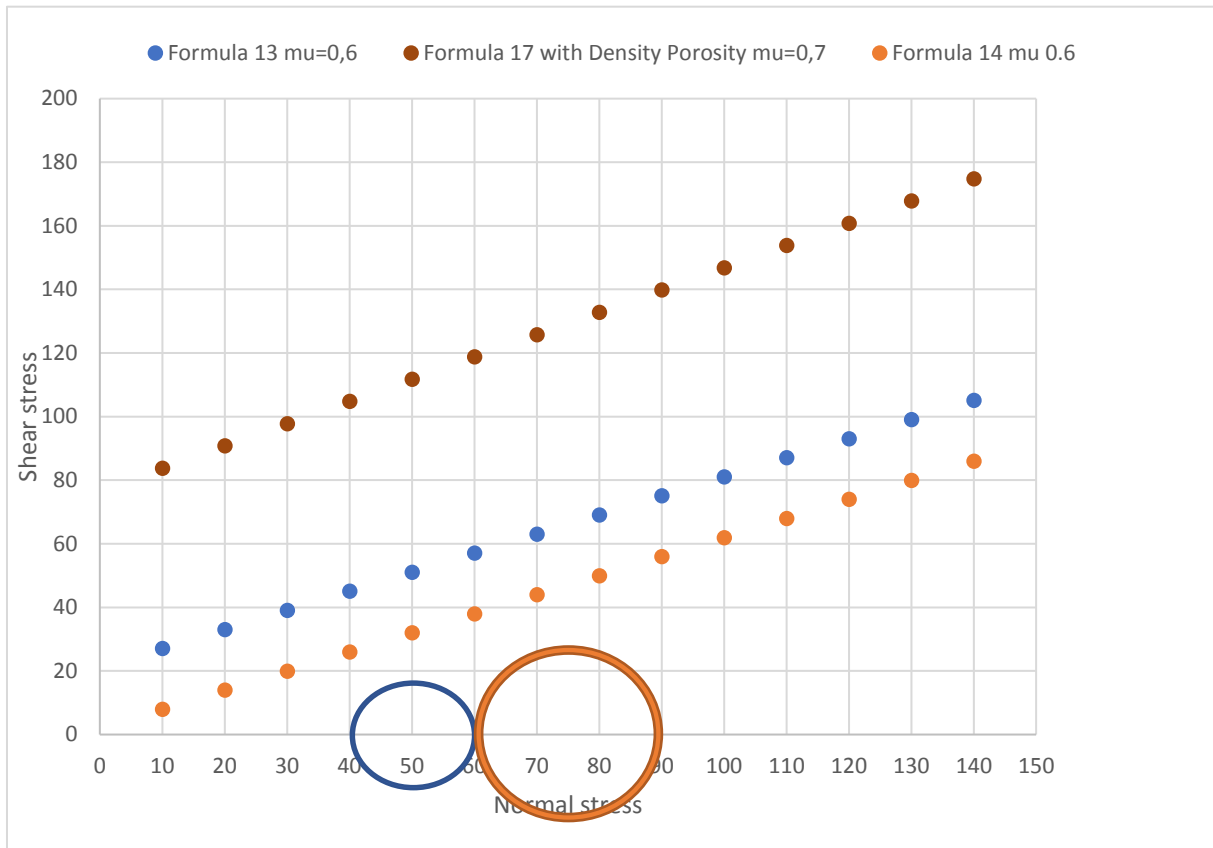
Figure 16 Failure envelopes with Mohr circles. Envelopes constructed with the failure criterion, using the UCSs calculated from Formula 13, 14 and 17 from Chang et al. (2006). Mohr Circles represent an extensional regime in blue and compressional regime in red using only overburden stress and the formulas of Rutqvist et al. (2008).

6.1.3. Discussion

A careful analysis of the Mohr circle in combination with the failure envelope needs to be made to determine the risk of rock failure in the reservoir rock. It is interesting to analyse the cap rock as well, but the next chapter on flexural bending is more suited for that. This follows from the non-varying character of the effective stress in cap rocks. Injection or production is located in the reservoir rock, so stress and pressure changes will occur in the reservoir rock as well. According to this calculation as seen in Figure 16, the reservoir rock is not close to failing. The Mohr circles have enough distance from the failure envelope of formula 13 with the weakest possible strength calculation. Even the improbable failure envelope of formula 14 is not intersecting with the Mohr circles, though they are closer to each other.

As for the other formulas, any formula which features unconsolidated sandstone is incorrect, because sandstone at a reservoir depth is consolidated. For this specific project a very clean sandstone is also an incorrect physical property on which to base the calculation. As this calculation is aimed at sandstones, a formula based on a conglomerate is also incorrect. These three properties are mentioned in formulas 9, 10, 11 and 17. Formula 17, based on a very clean sandstone, is still depicted in Figure 16 as it indicates the maximum strength a sandstone is likely to have, like formula 14 indicates the absolute minimum.

As the current stress regime present at the Cranberry Opportunity is unknown, both the compressional and extensional regimes are depicted. This is done to take every option into account. The used failure envelope and Mohr circle use the situation as it is at present. To calculate what is

likely to happen when either injection or production begins, the effective stress needs to be used. The effective stress is the resulting stress when the pore pressure is subtracted from the vertical and horizontal stresses. The effective stress is used because the overburden and horizontal stress will not vary, but the pore pressure will vary. The effective stress can incorporate the changing pore pressure in the Mohr circle. However when using effective stress to determine the Mohr circle, the failure envelope also needs to be constructed in terms of effective stress, using effective friction angle and effective cohesion. As these effective strength parameters are unknown, the 'effective' failure envelope cannot be constructed.

The Mohr circle on the other hand can be analysed more easily for effective stress using Haug *et al*. (2018). Formulas for calculating effective vertical and horizontal stress are listed therein, where v is the Poissons ratio and α is the Biot-Willis coefficient. An extensional regime is assumed.

19) $\Delta\sigma_h' = \left[\left(\frac{1-2v}{1-v}\right) - 1\right]\alpha\Delta P_f$

20) $\Delta\sigma_v' = -\alpha\Delta P_f$

A Poissons ratio of 0,3 and a Biot-Willis coefficient of 1 are used. σ_1 is 60 MPa and σ_3 is 40 MPa before injection or production. If the pore pressure is increased with 10 MPa due to injection, the effective horizontal stress is decreased with 4 MPa and the effective vertical stress with 10 MPa. In the case of production, pore pressure reduction, the effective stresses are increased by the same stresses, see Table 8. This implies that after injection the Mohr circle reduces in size and migrates to the left, after production the Mohr circle increases in size and migrates to the right.

	σ'_1 (MPa)	σ'_3 (MPa)	$\sigma'_1 - \sigma'_3$
Steady state	60	40	20
After injection	50	36	14
After production	70	44	26

Table 8 Overview of effective stresses after injection and production using Haug et al. (2018).

The comparison with the extensional stress regime Mohr circle is made in Figure 17. In both the injection and production case the Mohr circles don't touch the failure envelopes. It needs to be noted that the effective stresses are not based on an effective steady state stress and that the failure envelope is not based on effective stress. The figure is merely to show the movement and change in size of the Mohr circle. For a compressional regime the required effective stress formulas were not found, though the expectation is that the formulas will not deviate very much.
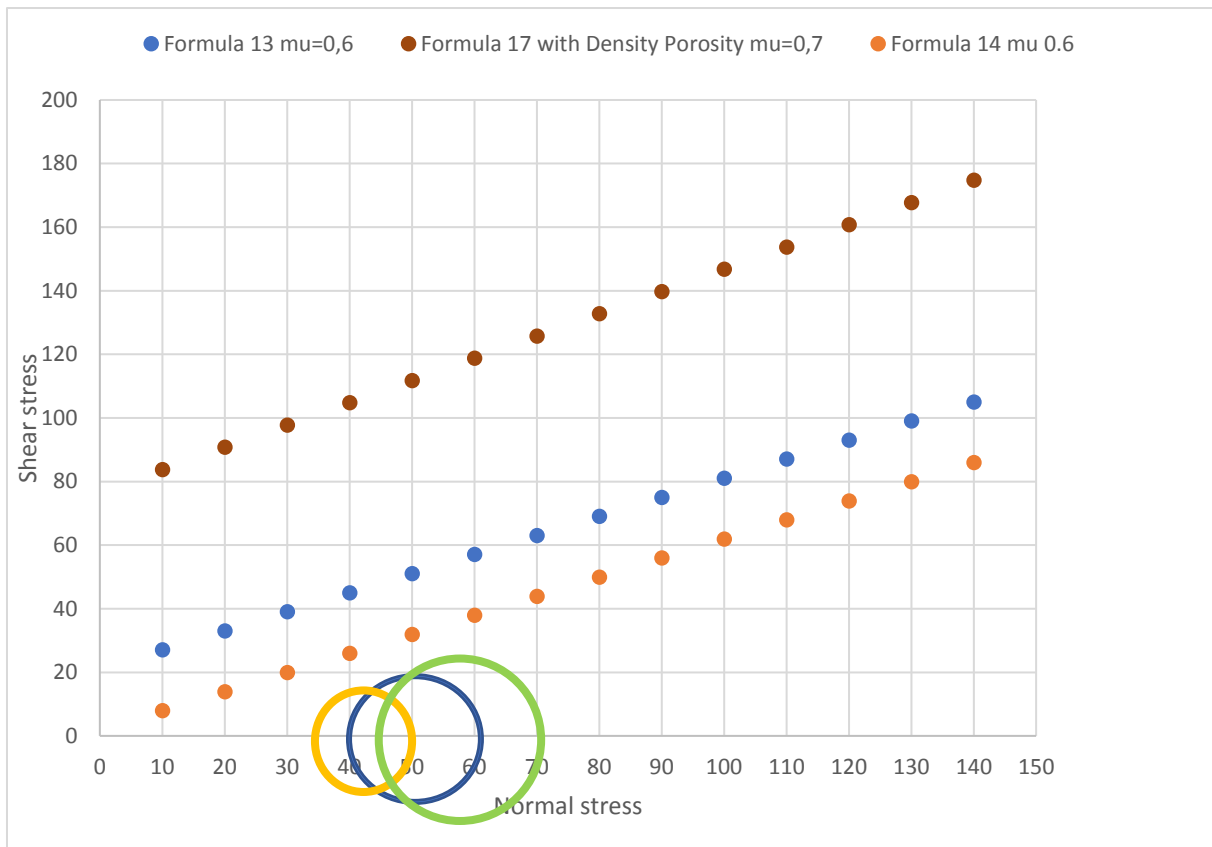
Figure 17 The failure envelopes using formulas 13, 14 and 17. The blue Mohr circle indicates the steady state, based on overpressure and an extensional regime. The yellow and green Mohr circle are calculated from the steady state non-effective stress. The yellow Mohr circle indicates the effective stress after injection and increasing the pore pressure with 10 MPa. The green Mohr circle indicate the effective stress state after production and decreasing the pore pressure with 10 MPa.

As the chance for rock failure while depleting is not significant in the first years, the expectation is that analyses on depleting circumstances will yield results that imply the same. Depletion would occur on the production side of the reservoir around the production well. It is expected that pressure redistribution might take some time, so it is still of interest to investigate that side of the reservoir in combination with injection. A new situation arises at the injection well as injection in a non-depleted reservoir has never been done. As pressure distribution is expected to not be instantaneous, the pore pressure build-up needs to be investigated. As the pore pressure rises, the effective stress decreases. It is advised to investigate the pressure distribution of the elevated pressure at the onset of injection with modelling, for example reactive transport modelling.

6.2. Reservoir compaction and cap rock flexural bending

Flexural bending in the case of a reservoir is the bending of the caprock due to compaction or bulging of a reservoir, which is caused by either producing its content or injecting substances. (Figure 18 (a) and (b)) This bending of the caprock will translate to the surface as land subsidence or bulging. The importance of investigating the potential for flexural bending lies in the development of tensile stresses at the bottom of the caprock while sagging. These stresses, when high enough, can cause micro fracturing in the caprock. This is not a problem with bulging, because it occurs at the top of the caprock, however in the case of sagging the natural gas in the reservoir can infiltrate into the caprock at the bottom. To determine the amount of bending the cap rock needs to be able to withstand, the maximum amount of compaction the reservoir can potentially sustain needs to be determined. The first part thus will be on a short look into reservoir compaction.
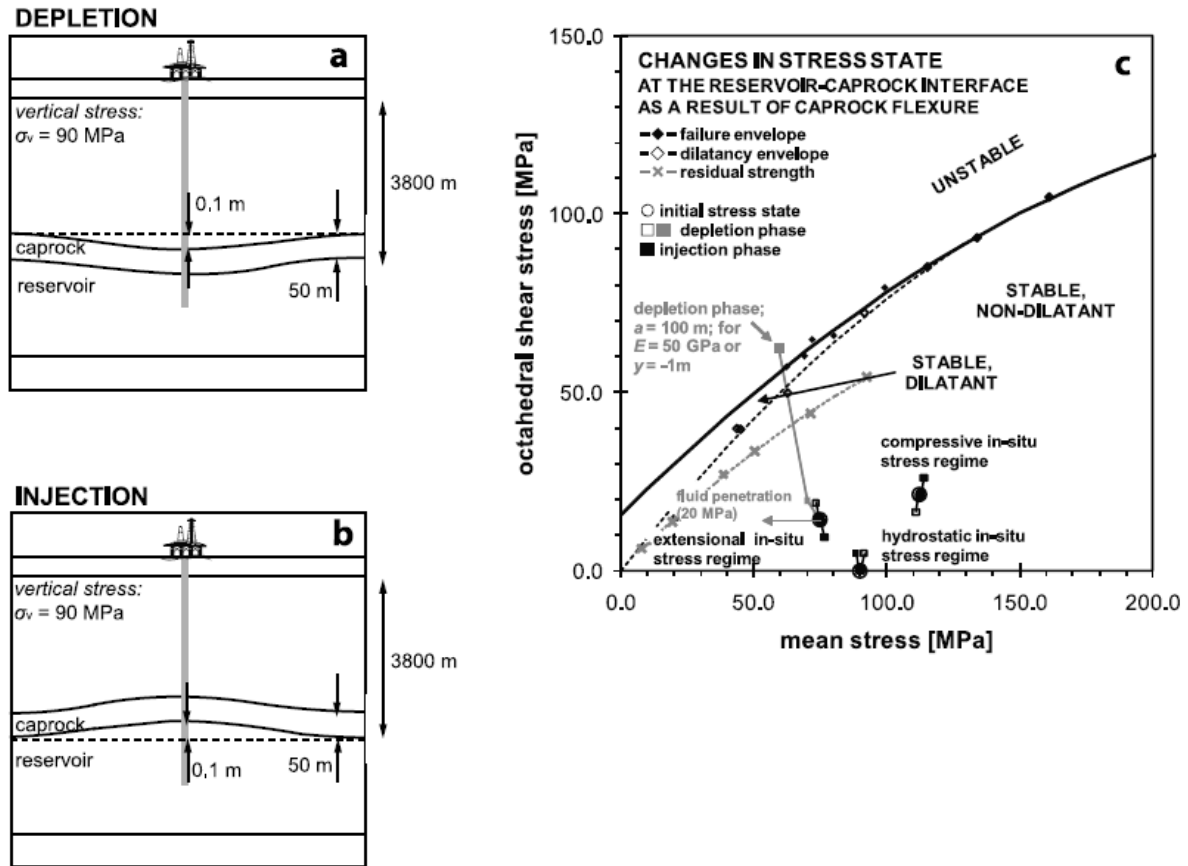
Figure 18 (a) Depletion and (b) injection scenarios for a hypothetical, circular reservoir-caprock system, with the reservoir-caprock interface at 3800 m depth. (c) Failure, dilatation, and residual strength envelopes for dry anhydrite under reservoir conditions (T = 80°C) combined with calculated depletion (open square, scenario a) and injection (solid square, scenario b) stress paths reflecting changes in stress at the base of the caprock, as a result of simple flexure of a caprock. Changes in stress state were calculated according to E = 5 GPa, y = ±10 cm, a = 100–5000 m and three different, initial, in situ stress regimes (center of open circle), assuming no fluid penetration. If penetration does occur, e.g., through permeability development, the effective mean stress will be reduced (e.g., for Pf = 20 MPa, see arrow in the extensional stress regime). Note that under the given conditions, no permeability development or caprock failure is to be expected, either during depletion or injection, with the exception of cases of highly localized compaction/heave (see solid square, for E = 50 GPa or y = −1 m, a = 100–5000 m). (Figure and caption taken from Hangx *et al.*, 2010)

6.2.1. Method for reservoir compaction

To determine the reservoir compaction several parameters are needed. The height of the reservoir is needed. The porosity of the reservoir rock is also needed. For maximum compaction a simple calculation can be performed that is based on the idea that all the pores will collapse so that there is no more porosity. This is not a real possibility, so this would be used to be on the absolute safe side of estimation. Mamora&Seo (2002) indicated that normal gas recovery from a gas field would be about 65% of the gas that is originally in place and conducted 1D experiments that with CO_2 injection this could exceed 70% and even almost reach 90%. To have a realistic estimation, the calculation will be done with 80% recovery. A simple calculation of the amount of compaction in a reservoir would be compaction=height*(porosity*recovery).
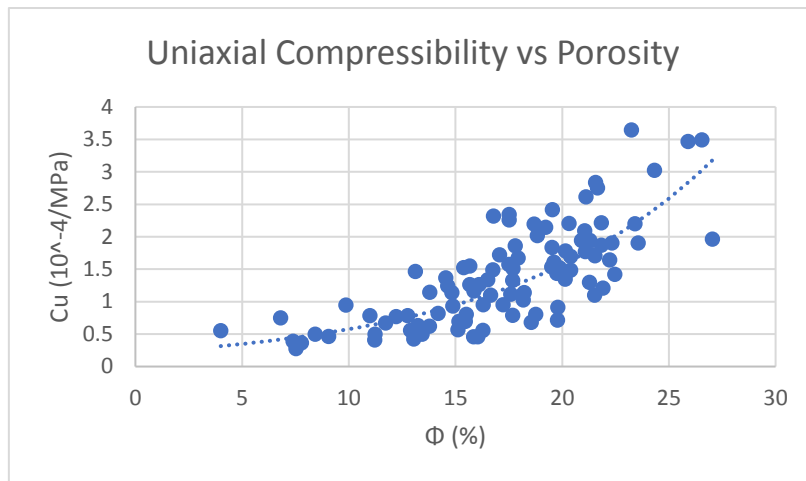
Figure 19 Uniaxial Compressibility against Porosity. Taken from Hettema et al. (2000)

To determine a more probable amount of compaction, the uniaxial compressibility of the reservoir is used. The uniaxial compressibility (1/MPa) (C_u) is determined $C_u = {-\Delta\varepsilon}/{\Delta p}$. If the porosity of a reservoir is known, Figure 19 can be used to determine the uniaxial compressibility of a reservoir. The planned change in pressure (p) in a reservoir can then be used to determine the change in strain (ε) of a reservoir. As strain is determine by $\varepsilon = {\Delta L}/{L_0}$, the calculated change in strain in combination with the height of the reservoir as L_0 can then be used to calculate the change in height and thus the amount of compaction.

Our case study doesn't have a uniform permeability and porosity. It has so called permeability streaks. To check if these permeability streaks have influence on the uniaxial compressibility and thus on the final amount of sagging of the caprock, nine scenarios of theoretical reservoirs were examined.

Porosity	5%	10%	15%	20%	Average porosity	C_u for average (See Figure 19)
Scenario 1	75		25		7.5	0.3
Scenario 2		90		10	11	0.6
Scenario 3	88.5		12.5		6.3	0.2
Scenario 4	88.5			12.5	6.9	0.2
Scenario 5		88.5	12.5		10.7	0.6
Scenario 6		88.5		12.5	11.4	0.6
Scenario 7		50		50	15	1
Scenario 8		75		25	12.5	0.8
Scenario 9		25		75	17.5	1.2

Table 9 Nine scenarios of different reservoirs.

As the scenario's depict reservoirs with permeability variations, imagine a two layered reservoir. There are then two options for calculating. The first is to take the porosities and the percentage of the reservoir with that porosity and calculate an average porosity for the whole reservoir and use that throughout the calculation starting at the determination of the uniaxial compressibility. The second option is to keep the multi-layered approach up until the start of the stress calculation to add up the compaction in both the layers. To determine the difference the different methods would garner, both were performed.

6.2.2. Results for reservoir compaction

As the reservoir has a height of 61 m and a porosity of 10%, the first calculation mentioned in 6.2.1 would be 61*(0.1*0.8)=4.9. The maximum compaction would be 4.9 m. According to Geertsema (1973) the ratio between depth and radius of a reservoir indicates the amount of subsidence that occurs with a specified amount of compaction. This is based on a circular shape. This ratio is described as η=D/R where D is depth and R is radius. A small and deep reservoir would hardly cause subsidence, even if there is noticeable compaction. An η of 1.0 and 0.2 were used to demonstrate this. The η=1.0 situation resulted in an amount of subsidence that was around 0.45 times the amount of compaction and the η=0.2 situation resulted in subsidence of about 1.2 times the compaction. Our case is best described as an ellipsoid shape, however if we use the length and thus increase the surface area, the estimate would be on the safe side. The length is 6842m, which results in a R of 3421 m. The depth is 2572 m. η=2572/3421 is 0.8. Next to the fact that it is highly likely that not all the compaction will translate to subsidence, this amount will still be unrealistically high. As stated in Van Thienen-Visser *et al.* (2015) the Groningen gas field with a thickness of around 100-300 m will yield a maximum amount of subsidence at the surface of 60 cm at the end of production. The η of the Groningen gas field will be 2600/22500=0.1. This suggests that the amount of subsidence is actually bigger than the amount of compaction, which implies that the amount of compaction in our case study is probably an order of magnitude smaller than 4.5 m. This because the Groningen gas field is thicker and can thus compact more.

The second calculation mentioned in 6.2.1 used the uniaxial compressibility. It is used for nine different scenarios with a change in pressure from 4-40 MPa. The results are showed in Figure 21. The amount of compaction with the highest amount of pressure change ranges from 5 mm to 3 cm.

To investigate a range of scenario's, 9 scenarios were determined to represent a range of potential reservoirs (see Table 9). As the example reservoir has so-called permeability streaks, this was incorporated in the potential reservoirs with a layering idea. The reservoirs consist of two layers which each have a different porosity. The results were calculated with an immediate averaging of the porosities of the different layers and using that porosity throughout the calculation. The results were also calculated where the layers remained separate and only in the final step of calculations the layers would be averaged. The differences between the results are small and one can choose either option in future calculations. (see Figure 20)
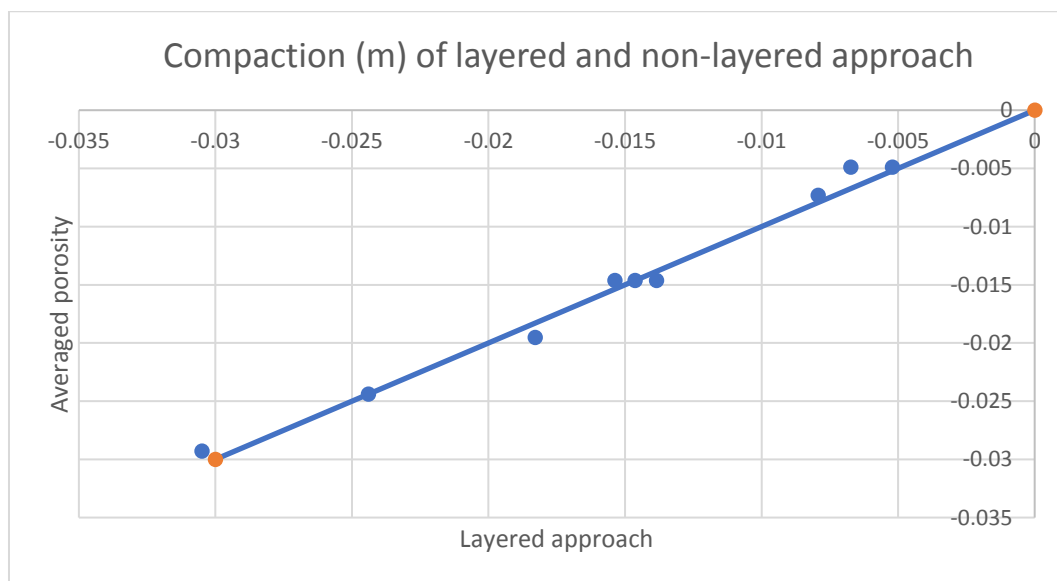

Figure 20 Comparing the two options of calculating compaction: layered or averaged out for all nine scenarios.
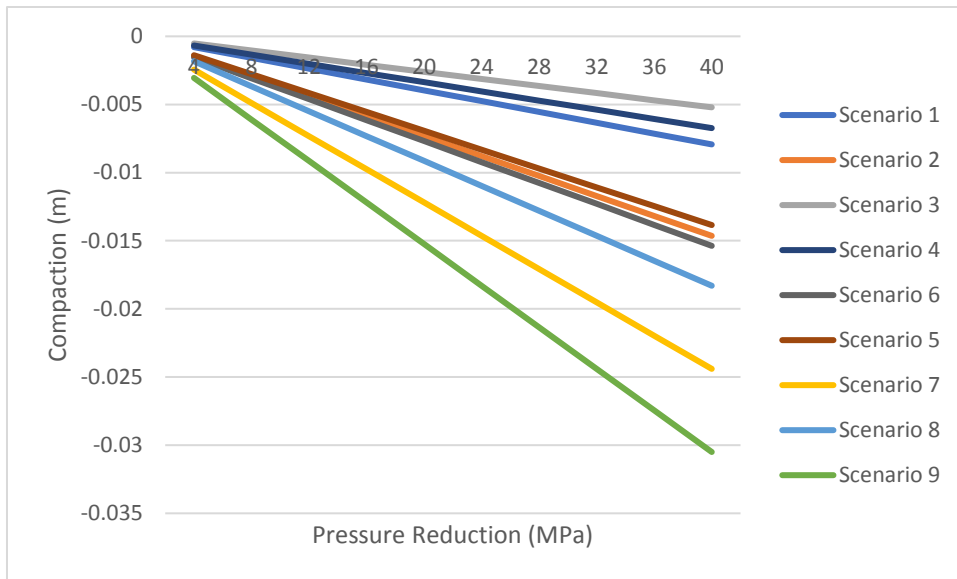
Figure 21 Amount of compaction (m) after reduction in pore pressure (MPa) in a layered situation.

6.2.3.   Method for cap rock flexural bending

To determine the potential for micro fractures, a model illustrating a field is used. The model can determine the stress that is working on the shape. The shape of the model can be either circular or ellipsoidal. In our example an ellipsoidal model is chosen. The example field Cranberry was found to be more ellipsoidal than circular. Then the formulas needed are to be determined. The formulas that are going to be used will need to contain the parameters stress and height difference in the centre. The height difference in the centre will illustrate the sagging or heaving of the cap rock. The stress parameter will give an indication of the changes in stress at the edge of the model and in the centre, and thus also in between. These stress changes can then be used in with the Mohr-Coulomb failure criterion mentioned in the previous section (6.1) to determine the effect the height difference will have on the stresses working on the model. This approach is chosen to simplify the natural situation. Every gas field has a different shape and to simplify calculations a generic shape close to the original is chosen, like a circle or an ellipse. The formulas used here are taken from Young&Budynas (2017). They are based on an ellipsoidal disk fixed at the sides with a uniform load and originate from material science. The sides are fixed as the caprock is located in between different rock layers. The sides are not able to move up- or downwards. The uniform load is linked to the overburden load that is homogeneous loading the caprock. Though the eventual caprock might not be homogeneous, it is assumed to be homogeneous to simplify the calculations. For a less simplified calculation, a layered approach can be tried. This layered approach might give better result, however this work will use the homogeneous approach as a layered approach might be more complicated than expected at first glance. The formulas used are listed in Figure 22. There are also formulas available for circular shapes in the work of Young&Budynas (2017). Because the caprock is bending, the Young's modulus and Poissons ratio needed are from the caprock and not the reservoir rock.

The cap rock in the North Sea area consist often either of shale or anhydrite. The Young's modulus and Poissons ratio for shale are taken from Horsrud *et al.* (1998) and for anhydrite they are taken form Hangx *et al.* (2010). From Horsrud *et al.* (1998) the shale samples taken into account are the Jurassic and Triassic shales from a depth similar to the depth of the cap rock at the project location

Cranberry, which is around 2000 m deep. The Young's modulus and Poissons ratio for shale are 2.4 GPa and 0.18 and for anhydrite 5 or 50 GPa and 0.25. Hangx *et al.* (2010) determined a Young's modulus around 50 GPa, however other modelling experiments used a modulus of an order of magnitude lower. This high Young's modulus is attributed to the rather pristine anhydrite sample used and an order of magnitude lower is used to represent a more probable Young's modulus.

	Shale	Anhydrite
Young's modulus	2.4 GPa	5 GPa
Poisson's ratio	0.18	0.25
Thickness layer	89	108
Inner radius	1237	1237
Outer radius	3421	3421
α	0.36	0.36

Table 10 Values used for this calculation. Radii are taken from the example field Cranberry.

First perform an analysis to determine the sensitivity on the results from the Young's modulus, the varying changes in height and the changes in uniform load. After this preliminary analysis of the sensitivity of the parameters, the compaction can be calculated, which then will be used to calculate an uniform load using a rewritten y_{max} formula. The uniform load can then be inserted into the stress formulas to generate the stress at various points in the cap rock.
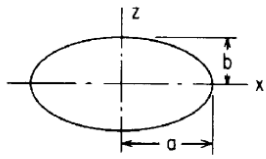
Configuration	Location	Equation
$\alpha = \frac{b}{a}$	At the edge of span a	$\sigma_x = \frac{6qb^2\alpha^2}{t^2(3+2\alpha^2+3\alpha^4)}$
	At the edge of span b	$\sigma_{max} = \sigma_z = \frac{6qb^2}{t^2(3+2\alpha^2+3\alpha^4)}$
	At the center	$\sigma_z = \frac{-3qb^2(1+v\alpha^2)}{t^2(3+2\alpha^2+3\alpha^4)}$ $\sigma_x = \frac{-3qb^2(\alpha^2+v)}{t^2(3+2\alpha^2+3\alpha^4)}$ $y_{max} = \frac{-3qb^4(1-v^2)}{2Et^3(3+2\alpha^2+3\alpha^4)}$

Symbol	Description	Unit
E	Elasic or Young's modulus	Pa
v	Poisson's ratio	-
σ	Bending stress	Pa
b	Inner radius of the ellipse	m
a	Outer radius of the ellipse	m
y_{max}	Maximum vertical deflection	m
q	Uniform load (force) per unit area	Pa
α	$\frac{b}{a}$	$-$
t	Thickness ellipse	m

Figure 22 Starting formulas and symbols used from Young&Budynas (2017)

6.2.4. Results for flexural bending

As scenario 5 is a good representation of the example field Cranberry, scenario 5 was used to calculate four different stresses, as shown in **Error! Reference source not found.**, using the formulas from Figure 22. For reference, scenario 3 and 9 were used as well to display the lowest and highest stress possible.
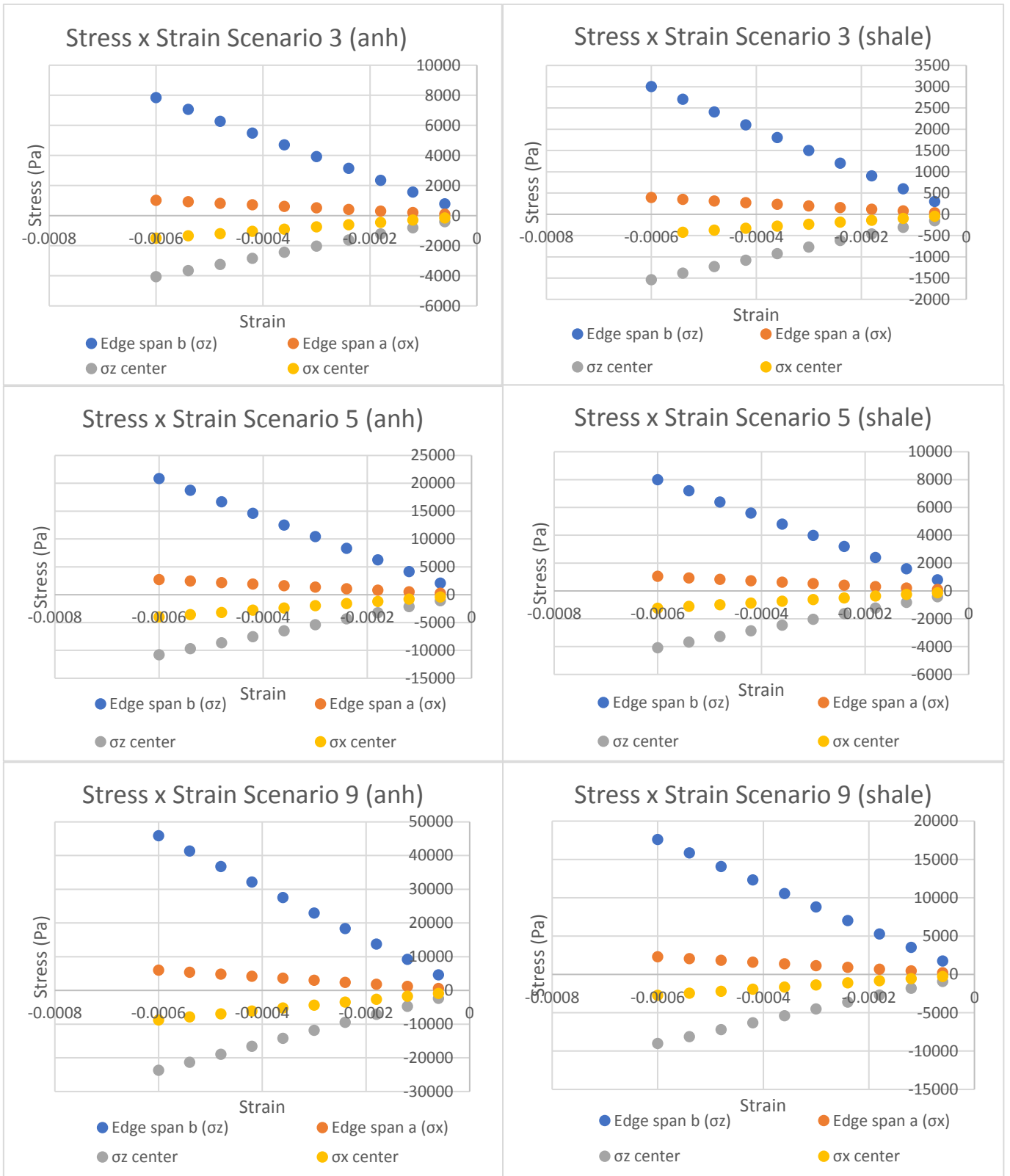
Figure 23 Stress strain curves for scenario 3, 5 and 9 for both a cap rock of anhydrite (anh) and shale. Scenario 3 has the lowest porosity and thus the lowest amount of compaction and thus lowest stress. Scenario 9 has the highest porosity and thus highest stress and scenario 5 is the closes to the Cranberry Opportunity.

The stresses shown in **Error! Reference source not found.** are abstract, Figure 24 shows where the stresses work. The calculated stresses are shown on Figure 24 (C) as the lower plane of the ellipse is

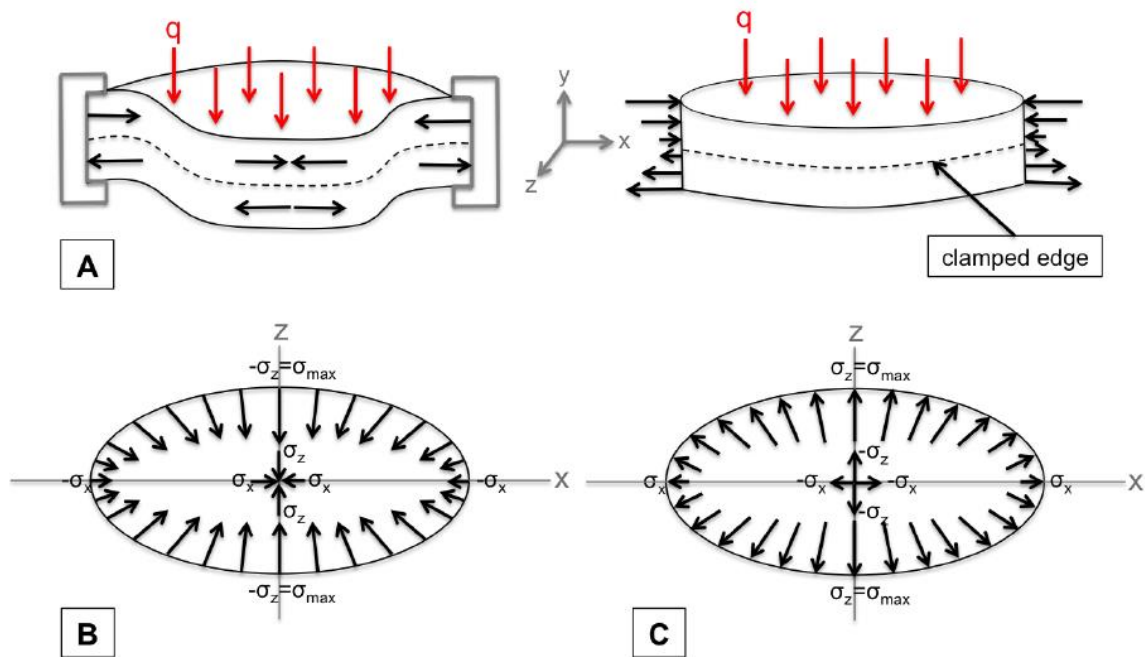where the stresses are working that might cause micro fractures.

Figure 24 A compilation of the stress directions and magnitudes in a clamped elliptical plate due to an uniform load (q). A) A cross-section (left) and an oblique side view of a clamped elliptical plate. The dotted line represents the unstressed neutral surface. B) A top view of the upper plane of the plate. C) A top view of the lower plane of the plate. (Fekkes (2016))

6.2.5. Discussion

The goal of looking into flexural bending was to determine if there is a possibility for micro fracturing to occur in the part of the reservoir where compaction occurs and to quantify mechanical effects. As the maximum deflection in the most extreme case is 3 cm, the probability of the development of micro fractures is small. Another argument to less fear micro fracture growth is that according to Hangx *et al*. (2010) the infiltration of CO_2 into the caprock is about 30 cm in 10000 years if the caprock consists mainly of anhydrite. Of course is this hypothetical, but nevertheless an indication of the limited effects of this infiltration. Note that the primary seal of the Cranberry reservoir is a shale and the secondary seal anhydrite. The second objective was to look into the changes in stress at the boundaries of the reservoir. As these stress changes are quite small, less than 0.02 MPa, the expectation is that these changes do not significantly influence the reservoir state of stress. To further demonstrate this, failure envelopes were constructed using the same method as used in paragraph 6.1 and the formulas listed in Table 11 taken from Chang *et al.* (2006). The Mohr circles were constructed using overburden stress and again both an extensional and compressional regime were displayed. The Mohr circles do not lie close to the failure envelopes. A movement from the Mohr circles of 0.02 MPa is not causing the circles to cross the failure envelope.
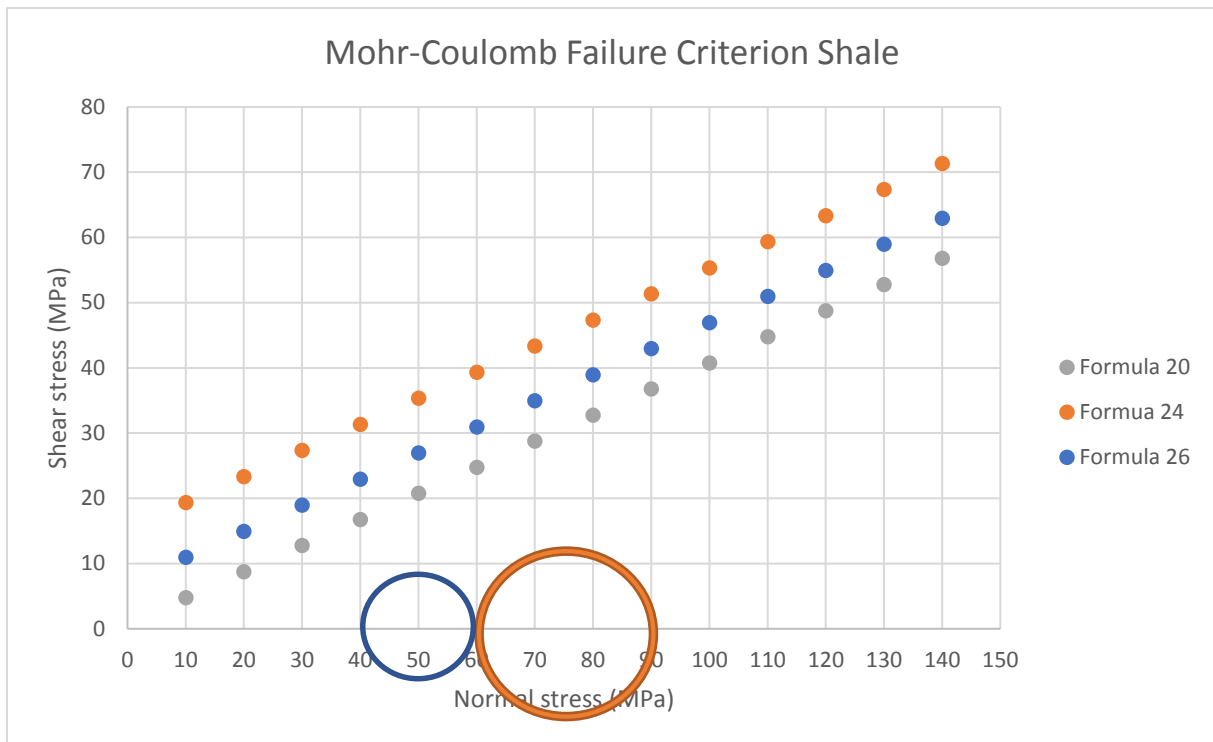
Figure 25 The failure criterion for shale. The UCS's used are calculated with formulas found in Chang et al. (2006). The Mohr circles are constructed using overburden stress, like in paragraph 6.1. An extensional regime is displayed with the blue circle and a compressional regime with the red circle.
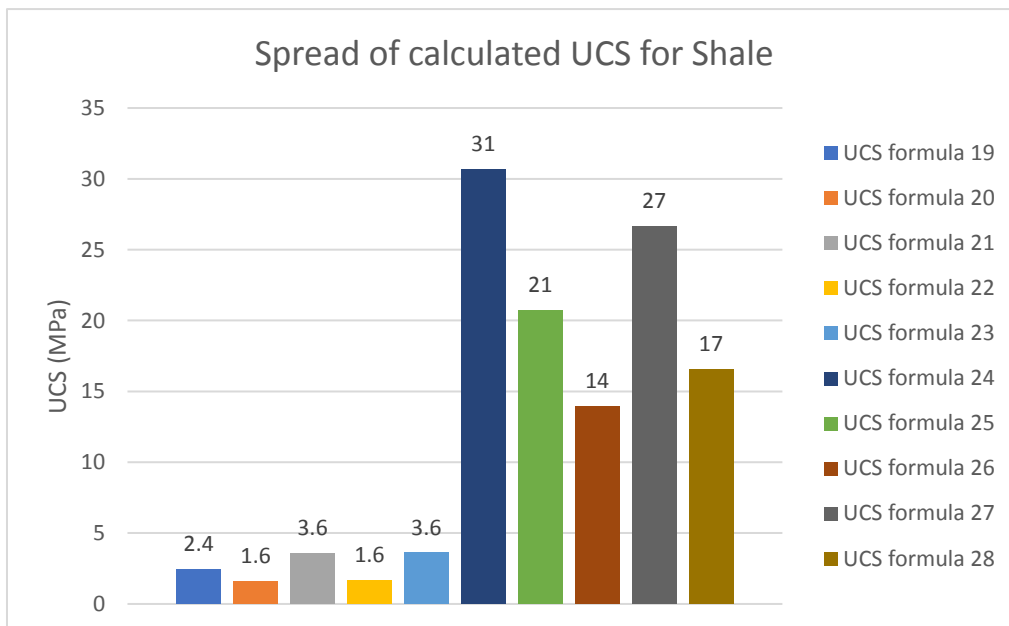

Figure 26 Spread of UCS's calculated with formulas listed in Table 11.

Eq. no.	UCS (MPa)	Origin	Comments	Reference
19	$0.77(304.8/\Delta t)2.93$	North Sea	Mostly high porosity Tertiary shales	Horsrud (2001)
20	$0.43(304.8/\Delta t)3.2$	Gulf of Mexico	Pliocene and younger	
21	$1.35(304.8/\Delta t)2.6$	Globally	-	
22	$0.5(304.8/\Delta t)3$	Gulf of Mexico	-	
23	$10(304.8/\Delta t - 1)$	North Sea	Mostly high porosity Tertiary	Lal (1999)

			shales	
24	$7.97E0.91$	North Sea	Mostly high porosity Tertiary shales	Horsrud (2001)
25	$7.22E0.712$	-	Strong and compacted shales	
26	$1.001\varphi - 1.143$	-	Low porosity ($\varphi < 0.1$) high strength ($\sim$ 79 MPa) shales	Lashkaripour& Dusseault (1993)
27	$2.922\varphi - 0.96$	North Sea	Mostly high porosity Tertiary shales	Horsrud (2001)
28	$0.286\varphi - 1.762$	-	High porosity ($\varphi > 0.27$) shales	

Table 11 Empirical relationships between unconfined compressive strength (UCS) and other physical properties in shale. If no reference is given, the formula is unpublished. (Table taken from Chang et al., 2006)

7. Summary and recommendations

Quite a bit of research has been aimed at the effects of CO_2 in a reservoir. Research aimed at chemical effects indicated the possible dissolution of minerals, though the speed of dissolution is slow. Also chemical dissolution depends on the presence of actual fluid for the minerals to dissolve into and the term fluid-rock ratio is important to remember. Research aimed at mechanical effects showed that CO_2 can cause both strengthening and weakening of a reservoir. In the case of the project Cranberry it is important to look at the strain caused by simultaneous injection and production. Another factor of interest will be the pressure and stress around the injection well at the onset of injection due to delayed pressure distribution. Hydrologically it is of interest if the CO_2 is injected into the aquifer. CO_2 can dissolve in an aquifer and the aquifer can then transport the CO_2 to unknown extent. CO_2 dissolution can also acidify fluid. Research aimed at porosity and permeability indicated both an increase and decrease. Increase of porosity and permeability was due to dissolution of minerals, decrease due to deposition of salts which would clog the permeability, for example around the injection well. As the Cranberry reservoir has permeability streaks and not a very high permeability, decrease of permeability is to be avoided. Quite a few of these effects can be researched with the help of reactive transport modelling and reservoir modelling. It is thus recommended to use these types of modelling to look for a more reservoir specific determination of the extent of above mentioned effects. The basic calculations performed in this work indicate that the reservoir is strong enough for injection and production and that flexural bending won't be a problem for the Cranberry reservoir. However the Mohr circles were determined with overburden stress and hypothetical formulas to translate the overburden stress to horizontal stress. If the actual stress state of the reservoir is known, it is advised to once more determine the Mohr circles and their relation to the constructed failure envelopes. In an optimal situation strength experiments on core samples will be performed to determine the failure envelope for this specific reservoir.

Potential effect	Expected to **not** play a role	Possibly plays a role	Expected to play a role	Further research recommended	Comments
Acidification of pore fluids			*		Pore fluid needs to be present
Dissolution of framework minerals			*	Yes	Extent depends on amount of pore fluid
Dissolution of cement (Anhydrite, calcite)			*	Yes	Extent depends on amount of pore fluid
Chemo-mechanical weakening of reservoir rock			*	Yes	
Precipitation of secondary minerals		*			
Salt precipitation		*			Pore fluid needs to be present
Clogging of pores		*		Yes	Pore fluid needs to be present
Chemo-mechanical weakening of cap rock	*				
Change state of stress			*	Yes	
(Re)Activating faults		*			
Onset of creep			*	Yes	
Reservoir compaction	*				
Flexural bending cap rock	*				
Fractures in the reservoir and caprock	*				
Joule-Thomson cooling	*				
Permeability increase of cap rock	*				

Table 12 Compact list of effects with expected effects.

8. Acknowledgements

9. References

Abdullah, W. S., Alshibli, K. A., & Al-Zou'bi, M. S. (1999). Influence of pore water chemistry on the swelling behavior of compacted clays. Applied Clay Science, 15(5–6), 447–462. https://doi.org/10.1016/S0169-1317(99)00034-4

Alkan, H., Cinar, Y., & Ülker, E. B. (2010). Impact of Capillary Pressure, Salinity and In situ Conditions on CO_2 Injection into Saline Aquifers. Transport in Porous Media, 84(3), 799–819. https://doi.org/10.1007/s11242-010-9541-8

André, L., Audigane, P., Azaroual, M., & Menjoz, A. (2007). Numerical modeling of fluid–rock chemical interactions at the supercritical CO_2–liquid interface during CO_2 injection into a carbonate reservoir, the Dogger aquifer (Paris Basin, France). Energy Conversion and Management, 48(6), 1782–1797. https://doi.org/10.1016/J.ENCONMAN.2007.01.006

André, L., Azaroual, M., & Menjoz, A. (2010). Numerical Simulations of the Thermal Impact of Supercritical CO_2 Injection on Chemical Reactivity in a Carbonate Saline Reservoir. Transport in Porous Media, 82(1), 247–274. https://doi.org/10.1007/s11242-009-9474-2

Bachu, S. (2008). CO_2 storage in geological media: Role, means, status and barriers to deployment. Progress in Energy and Combustion Science, 34(2), 254–273. https://doi.org/10.1016/J.PECS.2007.10.001

Bachu, S., & Bennion, B. (2008). Effects of in-situ conditions on relative permeability characteristics of CO_2-brine systems. Environmental Geology, 54(8), 1707–1722. https://doi.org/10.1007/s00254-007-0946-9

Baines, S. J., & Worden, R. H. (2001). Geological CO_2 disposal: Understanding the long-term fate of CO_2 in naturally occurring accumulations. In Fifth International Conference on Greenhouse Gas Control Technologies, Cairns, CSIRO, Collingwood (pp. 311–316).

Bielinski, A., Kopp, A., Schütt, H., & Class, H. (2008). Monitoring of CO_2 plumes during storage in geological formations using temperature signals: Numerical investigation. International Journal of Greenhouse Gas Control, 2(3), 319–328. https://doi.org/10.1016/J.IJGGC.2008.02.008

Brady, P. V, & Walther, J. V. (1990). Kinetics of quartz dissolution at low temperatures. Chemical Geology, 82, 253–264. https://doi.org/https://doi.org/10.1016/0009-2541(90)90084-K

Busch, A., Kampman, N., Hangx, S. J., Snippe, J., Bickle, M., Bertier, P., … Schaller, M. (2014). The Green River Natural Analogue as A Field Laboratory To Study the Long-term Fate of CO_2 in the subsurface. Energy Procedia, 63, 2821–2830. https://doi.org/10.1016/J.EGYPRO.2014.11.304

Chalbaud, C., Robin, M., Lombard, J.-M., Martin, F., Egermann, P., & Bertin, H. (2009). Interfacial tension measurements and wettability evaluation for geological CO2 storage. Advances in Water Resources, 32(1), 98–109. https://doi.org/10.1016/J.ADVWATRES.2008.10.012

Chang, C., Zoback, M. D., & Khaksar, A. (2006). Empirical relations between rock strength and physical properties in sedimentary rocks. Journal of Petroleum Science and Engineering, 51(3–4), 223–237. https://doi.org/10.1016/J.PETROL.2006.01.003

Deere, D. U., & Miller, R. P. (1966). Engineering classification and index properties for intact rock. Illinois Univ At Urbana Dept Of Civil Engineering.

Duan, Z., & Sun, R. (2003). An improved model calculating CO2 solubility in pure water and aqueous NaCl solutions from 273 to 533 K and from 0 to 2000 bar. Chemical Geology, 193(3–4), 257–271. https://doi.org/10.1016/S0009-2541(02)00263-2

Duan, Z., Sun, R., Zhu, C., & Chou, I.-M. (2006). An improved model for the calculation of CO2 solubility in aqueous solutions containing Na+, K+, Ca2+, Mg2+, Cl−, and SO42−. Marine Chemistry, 98(2–4), 131–139. https://doi.org/10.1016/J.MARCHEM.2005.09.001

Duveau, G., Shao, J. F., & Henry, J. P. (1998). Assessment of some failure criteria for strongly anisotropic geomaterials. Mechanics of Cohesive-frictional Materials: An International Journal on Experiments, Modelling and Computation of Materials and Structures, 3(1), 1–26.

Fekkes, F. (2016). Field data correlation of reservoir compaction and seismic potential of Dutch onshore gas fields. Utrecht University.

Fjar, E., Holt, R. M., Raaen, A. M., Risnes, R., & Horsrud, P. (2008). Petroleum related rock mechanics (Vol. 53). Elsevier.

Freyburg, E. (1972). Der Untere und mittlere Buntsandstein SW-Thuringen in seinen gesteinstechnicschen Eigenschaften. Deustche Gesellschaft Geologische Wissenschaften. A; Berlin, 176, 911–919.

Fuller, R. C., Prevost, J. H., & Piri, M. (2006). Three-phase equilibrium and partitioning calculations for CO2 sequestration in saline aquifers. Journal of Geophysical Research: Solid Earth, 111(B6). https://doi.org/10.1029/2005JB003618

Gaus, I. (2010). Role and impact of CO2–rock interactions during CO2 storage in sedimentary rocks. International Journal of Greenhouse Gas Control, 4(1), 73–89. https://doi.org/10.1016/J.IJGGC.2009.09.015

Geertsma, J. (1973). Land subsidence above compacting oil and gas reservoirs. Journal of Petroleum Technology, 25(06), 734–744.

Giorgis, T., Carpita, M., & Battistelli, A. (2007). 2D modeling of salt precipitation during the injection of dry CO2 in a depleted gas reservoir. Energy Conversion and Management, 48(6), 1816–1826. https://doi.org/10.1016/J.ENCONMAN.2007.01.012

Hangx, S. J. T., Spiers, C. J., & Peach, C. J. (2010). Creep of simulated reservoir sands and coupled chemical-mechanical effects of CO2 injection. Journal of Geophysical Research: Solid Earth, 115(B9). https://doi.org/10.1029/2009JB006939

Hangx, S. (2005, December 1). Subsurface mineralisation. Rate of CO2 mineralisation and geomechanical effects on host and seal formations. Behaviour of the CO2-H2O system and

preliminary mineralisation model and experiments. Retrieved from
https://inis.iaea.org/search/search.aspx?orig_q=RN:38004384

Hangx, S. (2005, March 1). Subsurface mineralisation. Rate of CO2 mineralisation and geomechanical
effects on host and seal formations. A review of relevant reactions and reaction rate data. First
interim report. Retrieved from https://inis.iaea.org/search/search.aspx?orig_q=RN:42020972

Hangx, S. J. T. (2006). Subsurface mineralisation: Rate of CO2 mineralisation and geomechanical
effects on host and seal formations Reactions, reaction rates and porosity-permeability models for
CO2 injected sandstone rocks.

Hangx, S., Bakker, E., Bertier, P., Nover, G., & Busch, A. (2015). Chemical–mechanical coupling
observed for depleted oil reservoirs subjected to long-term CO2-exposure – A case study of the
Werkendam natural CO2 analogue field. Earth and Planetary Science Letters, 428, 230–242.
https://doi.org/10.1016/J.EPSL.2015.07.044

Hangx, S., van der Linden, A., Marcelis, F., & Bauer, A. (2013). The effect of CO2 on the mechanical
properties of the Captain Sandstone: Geological storage of CO2 at the Goldeneye field (UK).
International Journal of Greenhouse Gas Control, 19, 609–619.
https://doi.org/10.1016/J.IJGGC.2012.12.016

Haug, C., Henk, A., & Nüchter, J.-A. (2017). Numerical modelling of production-induced stress
changes and fault reactivation in Rotliegend gas fields of the North German Basin.
https://doi.org/10.3997/2214-4609.201701681

Heinemann, N., Wilkinson, M., Haszeldine, R. S., Fallick, A. E., & Pickup, G. E. (2013). CO2
sequestration in a UK North Sea analogue for geological carbon storage. Geology, 41(4), 411–414.
Retrieved from http://dx.doi.org/10.1130/G33835.1

Hendry, J. P., Wilkinson, M., Fallick, A. E., & Haszeldine, R. S. (2000). Ankerite Cementation in Deeply
Buried Jurassic Sandstone Reservoirs of the Central North Sea. Journal of Sedimentary Research,
70(1), 227–239. Retrieved from http://dx.doi.org/10.1306/2DC4090D-0E47-11D7-
8643000102C1865D

Hettema, M.H.H., Schutjens, P.M.T.M., Verboom, B.J.M., Gussinklo, H. J. (2000). Production-Induced
Compaction of a Sandstone Reservoir: The Strong Influence of Stress Path. SPE Reservoir Evaluation
& Engineering, 3(04). https://doi.org/https://doi.org/10.2118/65410-PA

Hol, S., van der Linden, A. J., Zuiderwijk, P. M. M., Marcelis, F. H. M., & Coorn, A. H. (2015).
Mechanical characterization of Permian reservoir sandstone from the Moddergat-3 well in the Dutch
Wadden Area.

Horsrud, P., SØnstebØ, E. F., & BØe, R. (1998). Mechanical and petrophysical properties of North Sea
shales. International Journal of Rock Mechanics and Mining Sciences, 35(8), 1009–1020.
https://doi.org/https://doi.org/10.1016/S0148-9062(98)00162-4

Horsrud, P. (2001). Estimating mechanical properties of shale from empirical correlations. SPE Drilling
& Completion, 16(02), 68–73.

HOWER, J., ESLINGER, E. V, HOWER, M. E., & PERRY, E. A. (1976). Mechanism of burial
metamorphism of argillaceous sediment: 1. Mineralogical and chemical evidence. GSA Bulletin, 87(5),
725–737. Retrieved from http://dx.doi.org/10.1130/0016-
7606(1976)87%3C725:MOBMOA%3E2.0.CO

Huang, W. L., Bishop, A. M., & Brown, R. W. (1986). The effect of fluid/rock ratio on feldspar dissolution and illite formation under reservoir conditions. Clay Minerals (Vol. 21).

Hurter, S., Berge, J. G., Labregere, D. (2007). Simulations for CO2 injection projects with Compositional Simulator. Offshore Europe, (January).

Jaeger, J. C., Cook, N. G. W., & Zimmerman, R. (2009). Fundamentals of rock mechanics. John Wiley & Sons.

Jennings, S., & Thompson, G. R. (1986). Diagenesis of Plio-Pleistocene sediments of the Colorado River delta, Southern California. Journal of Sedimentary Research, 56(1), 89–98. Retrieved from http://dx.doi.org/10.1306/212F8891-2B24-11D7-8648000102C1865D

Kaszuba, J. P., Janecky, D. R., & Snow, M. G. (2003). Carbon dioxide reaction processes in a model brine aquifer at 200 °C and 200 bars: implications for geologic sequestration of carbon. Applied Geochemistry, 18(7), 1065–1080. https://doi.org/10.1016/S0883-2927(02)00239-1

Kaszuba, J. P., Janecky, D. R., & Snow, M. G. (2005). Experimental evaluation of mixed fluid reactions between supercritical carbon dioxide and NaCl brine: Relevance to the integrity of a geologic carbon repository. Chemical Geology, 217(3), 277–293. https://doi.org/https://doi.org/10.1016/j.chemgeo.2004.12.014

Kleinitz, W., Dietzsch, G., & Köhler, M. (2003). Halite Scale Formation in Gas-Producing Wells. Chemical Engineering Research and Design, 81(3), 352–358. https://doi.org/10.1205/02638760360596900

Kohli, A. H., & Zoback, M. D. (2013). Frictional properties of shale reservoir rocks. Journal of Geophysical Research: Solid Earth, 118(9), 5109–5125. https://doi.org/10.1002/jgrb.50346

Lal, M. (1999). Shale stability: drilling fluid interaction and shale strength. In SPE Asia Pacific Oil and Gas Conference and Exhibition. Society of Petroleum Engineers.

Lashkaripour, G. R., & Duseault, M. B. (1993). A statistical study on shale properties: Relationship among principal shale properties. In PMGE, Australia, Probalistic Method in Geotechnical Engineering.

Liteanu, E., & Spiers, C. J. (2009). Influence of pore fluid salt content on compaction creep of calcite aggregates in the presence of supercritical CO2. Chemical Geology, 265(1–2), 134–147. https://doi.org/10.1016/J.CHEMGEO.2008.12.010

Lokhorst, A. (1998). The Northwest European gasatlas. Netherlands Institute of Applied Geoscience TNO (Haarlem). ISBN 90-72869-60-5.

Mamora, D. D., & Seo, J. G. (2002). Enhanced gas recovery by carbon dioxide sequestration in depleted gas reservoirs. In SPE Annual Technical Conference and Exhibition. Society of Petroleum Engineers.

Marbler, H., Erickson, K. P., Schmidt, M., Lempp, C., & Pöllmann, H. (2013). Geomechanical and geochemical effects on sandstones caused by the reaction with supercritical CO2: an experimental approach to in situ conditions in deep geological reservoirs. Environmental Earth Sciences, 69(6), 1981–1998. https://doi.org/10.1007/s12665-012-2033-0

Mathias, S. A., de Miguel, G. J., Thatcher, K. E., & Zimmerman, R. W. (2011). Pressure Buildup During CO2 Injection into a Closed Brine Aquifer. Transport in Porous Media, 89(3), 383–397. https://doi.org/10.1007/s11242-011-9776-z

Mathias, S. A., Hardisty, P. E., Trudell, M. R., & Zimmerman, R. W. (2008). Approximate Solutions for Pressure Buildup During CO2 Injection in Brine Aquifers. Transport in Porous Media, 79(2), 265. https://doi.org/10.1007/s11242-008-9316-7

Mathias, S. A., Hardisty, P. E., Trudell, M. R., & Zimmerman, R. W. (2009). Screening and selection of sites for CO2 sequestration based on pressure buildup. International Journal of Greenhouse Gas Control, 3(5), 577–585. https://doi.org/https://doi.org/10.1016/j.ijggc.2009.05.002

McNally, G. . (1987). Estimation of coal measures rock strength using sonic and neutron logs. Geoexploration, 24(4–5), 381–395. https://doi.org/10.1016/0016-7142(87)90008-1

Miri, R., van Noort, R., Aagaard, P., & Hellevang, H. (2015). New insights on the physics of salt precipitation during injection of CO2 into saline aquifers. International Journal of Greenhouse Gas Control, 43, 10–21. https://doi.org/https://doi.org/10.1016/j.ijggc.2015.10.004

Moos, D., Zoback, M. D., & Bailey, L. (2001). Feasibility Study of the Stability of Openhole Multilaterals, Cook Inlet, Alaska. SPE Drilling & Completion, 16(03), 140–145. https://doi.org/10.2118/73192-PA

Nover, G., von der Gönna, J., Heikamp, S., & Köster, J. (2013). Changes of petrophysical properties of sandstones due to interaction with supercritical carbon dioxide – a laboratory study. European Journal of Mineralogy, 25(3), 317–329. Retrieved from http://dx.doi.org/10.1127/0935-1221/2013/0025-2295

Oldenburg, C. M. (2007). Joule-Thomson cooling due to CO2 injection into natural gas reservoirs. Energy Conversion and Management, 48(6), 1808–1815. https://doi.org/10.1016/J.ENCONMAN.2007.01.010

Pruess, K., & Müller, N. (2009). Formation dry-out from CO 2 injection into saline aquifers: 1. Effects of solids precipitation and their mitigation. Water Resources Research, 45(3). https://doi.org/10.1029/2008WR007101

Rathnaweera, T. D., Ranjith, P. G., Perera, M. S. A., Haque, A., Lashin, A., Al Arifi, N., … Yasar, E. (2015). CO2-induced mechanical behaviour of Hawkesbury sandstone in the Gosford basin: An experimental study. Materials Science and Engineering: A, 641, 123–137. https://doi.org/10.1016/J.MSEA.2015.05.029

Ren, Q.-Y., Chen, G.-J., Yan, W., & Guo, T.-M. (2000). Interfacial tension of (CO2+ CH4)+ water from 298 K to 373 K and pressures up to 30 MPa. Journal of Chemical & Engineering Data, 45(4), 610–612.

Rimmelé, G., Barlet-Gouédard, V., & Renard, F. (2010). Evolution of the Petrophysical and Mineralogical Properties of Two Reservoir Rocks Under Thermodynamic Conditions Relevant for CO2 Geological Storage at 3 km Depth. Oil Gas Sci. Technol. – Rev. IFP, 65(4), 565–580. https://doi.org/10.2516/ogst/2009071

Rochelle, C. A., Czernichowski-Lauriol, I., & Milodowski, A. E. (2004). The impact of chemical reactions on CO_2 storage in geological formations: a brief review. Geological Society, London, Special Publications, 233(1), 87. Retrieved from http://sp.lyellcollection.org/content/233/1/87.abstract

Rohmer, J., Pluymakers, A., & Renard, F. (2016). Mechano-chemical interactions in sedimentary rocks in the context of CO2 storage: Weak acid, weak effects? Earth-Science Reviews, 157, 86–110. https://doi.org/10.1016/J.EARSCIREV.2016.03.009

Rosenbauer, R. J., Koksalan, T., & Palandri, J. L. (2005). Experimental investigation of CO2–brine–rock interactions at elevated temperature and pressure: Implications for CO2 sequestration in deep-saline aquifers. Fuel Processing Technology, 86(14–15), 1581–1597. https://doi.org/10.1016/J.FUPROC.2005.01.011

Rutqvist, J., Birkholzer, J. T., & Tsang, C.-F. (2008). Coupled reservoir–geomechanical analysis of the potential for tensile and shear failure associated with CO2 injection in multilayered reservoir–caprock systems. International Journal of Rock Mechanics and Mining Sciences, 45(2), 132–143. https://doi.org/10.1016/J.IJRMMS.2007.04.006

Santema, P. A. (2017, September 27). Grote gasvondst bij Schiermonnikoog. Dagblad van Het Noorden.

SciMed. (n.d.). What is Supercritical CO2 Extraction? Retrieved October 19, 2018, from https://www.scimed.co.uk/supercritical-co2-extraction/

Torp, T. A., & Gale, J. (2004). Demonstrating storage of CO2 in geological reservoirs: The Sleipner and SACS projects. Energy, 29(9–10), 1361–1369. https://doi.org/10.1016/J.ENERGY.2004.03.104

Ülker, E. B. (2009). Investigation of the CO2 storage capacity of aquifer structures: CO2 storage in a Buntsandstein prototype aquifer. Clausthal University of Technology, Germany.

Ullah, W. (2015). Mohr-Coulomb shear failure criterion. Retrieved October 4, 2018, from https://www.slideshare.net/wajahatullah8/lecture-11-shear-strength-of-soil-ce240

United Nations Treaty Collect. Paris Agreement (2015). Paris: United Nations.

Usdowski, H.-E. (1968). The Formation of Dolomite in Sediments. In G. Müller & G. M. Friedman (Eds.), Recent Developments in Carbonate Sedimentology in Central Europe (pp. 21–32). Berlin, Heidelberg: Springer Berlin Heidelberg.

Van der Linden, A. J., Zuiderwijk, P. M. M., Hol, S., Marcelis, F., & Coorn, A. H. (2015). Geomechanical experiments on Ten Boer rock samples from well Moddergat-3. Rijswijk: NAM.

Van Eijs, R. M. H. E., Mulders, F. M. M., Nepveu, M., Kenter, C. J., & Scheffers, B. C. (2006). Correlation between hydrocarbon reservoir properties and induced seismicity in the Netherlands. Engineering Geology, 84(3–4), 99–111. https://doi.org/10.1016/J.ENGGEO.2006.01.002

van Thienen-Visser, K., Pruiksma, J. P., & Breunese, J. N. (2015). Compaction and subsidence of the Groningen gas field in the Netherlands. Proceedings of the International Association of Hydrological Sciences, 372, 367–373.

Vernik, L., Bruno, M., & Bovberg, C. (1993). Empirical relations between compressive strength and porosity of siliciclastic rocks. International Journal of Rock Mechanics and Mining Sciences & Geomechanics Abstracts, 30(7), 677–680. https://doi.org/10.1016/0148-9062(93)90004-W

W. Johnson, J., Nitao, J., & Morris, J. (2004). Reactive Transport Modeling of Cap Rock Integrity During Natural and Engineered CO2 Storage. Carbon Dioxide Capture for Storage in Deep Geologic Formations, 2.

Wiebes, E. D. (2018, May 30). Gaswinning uit de kleine velden in de energietransitie. Letter to Parliament, p. 13.

Wilkinson, M., Haszeldine, R. S., Fallick, A. E., Odling, N., Stoker, S. J., & Gatliff, R. W. (2009). CO2–Mineral Reaction in a Natural Analogue for CO2 Storage—Implications for Modeling. Journal of Sedimentary Research, 79(7), 486–494. Retrieved from http://dx.doi.org/10.2110/jsr.2009.052

Wong, T. E., Batjes, D. A. J., & de Jager, J. (2007). Geology of the Netherlands. Edita-the Publishing House of the Royal.

Young, W. C., Budnyas, R. G. (2017). Roark's formulas for stress and strain. (Seventh). McGraw-Hill.